THE JOURNAL OF BIOLOGICAL CHEMISTRY VOL. 291, NO. 21, pp. 11252–11267, May 20, 2016

Functional and Structural Characterization of Bub3·BubR1 Interactions Required for Spindle Assembly Checkpoint Signaling in Human Cells*

Received for publication, November 2, 2015, and in revised form, February 29, 2016 Published, JBC Papers in Press, March 30, 2016, DOI 10.1074/jbc.M115.702142

Florian Prinz[‡1], Vera Puetter[§], Simon J. Holton[§], Dorothee Andres[§], Christian M. Stegmann[§], Dennis Kwiatkowski[§], Stefan Prechtl[§], Kirstin Petersen[‡], Georg Beckmann[¶], Bertolt Kreft[‡], Dominik Mumberg[‡], and Amaury Fernández-Montalván[§2]

From [§]Lead Discovery, [¶]Target Discovery, and [‡]TRG Oncology, Bayer Pharma AG, Global Drug Discovery, 13353 Berlin, Germany

The spindle assembly checkpoint (SAC) is an essential safeguarding mechanism devised to ensure equal chromosome distribution in daughter cells upon mitosis. The proteins Bub3 and BubR1 are key components of the mitotic checkpoint complex, an essential part of the molecular machinery on which the SAC relies. In the present work we have performed a detailed functional and biochemical characterization of the interaction between human Bub3 and BubR1 in cells and *in vitro*. Our results demonstrate that genetic knockdown of Bub3 abrogates the SAC, promotes apoptosis, and inhibits the proliferation of human cancer cells. We also show that the integrity of the human mitotic checkpoint complex depends on the specific recognition between BubR1 and Bub3, for which the BubR1 Gle2 binding sequence motif is essential. This 1:1 binding event is high affinity, enthalpy-driven and with slow dissociation kinetics. The affinity, kinetics, and thermodynamic parameters of the interaction are differentially modulated by small regions in the N and C termini of the Gle2 binding domain sequence, suggesting the existence of "hotspots" for this protein-protein interaction. Furthermore, we show that specific disruption of endogenous BubR1·Bub3 complexes in human cancer cells phenocopies the effects observed in gene targeting experiments. Our work enhances the current understanding of key members of the SAC and paves the road for the pursuit of novel targeted cancer therapies based on SAC inhibition.

During mitosis, the spindle assembly checkpoint (SAC)[3] ensures that newly replicated chromosomes are distributed equally in daughter cells. Loss of SAC activity results in aneuploidy and chromosomal instability, both considered to be hallmarks of cancer (1). At metaphase, all chromosomes must attach in a bi-oriented fashion to the spindle microtubule at each sister kinetochore pair and attain equal tension at the spindle equator before the commencement of anaphase separation. Unattached or tensionless kinetochores trigger the SAC, which results in the production of the mitotic checkpoint complex (MCC). The MCC, which contains the proteins Mad2, BubR1, and Bub3, forms an inhibitory complex with Cdc20 (2, 3). Cdc20 is an essential cofactor for the anaphase promoting complex, or cyclosome (APC/C), an E3 ligase that targets proteins like mitotic cyclins for proteolytic degradation. Hence, inhibition of Cdc20 results in delay of anaphase onset. A lack of Bub3 or other components of the MCC leads to mitotic failures with severe chromosome segregation defects and cell death (4–7).

Bub3 is a "donut-shaped" WD40 protein with a seven-blade β-propeller structure forming a symmetric circular wall around a central pore or funnel region (8, 9). It binds to phosphorylated MELT repeats (Met-Glu-Leu-Thr(P)) on the outer kinetochore subunit Knl1, acting as a scaffolding protein for its binding partners BubR1 and Bub1 (10–15). The interaction with these two proteins takes place via the Bub3 central pore region and the Gle2 binding sequence (GLEBS) motif of BubR1/Bub1, respectively (16). In both complexes, the GLEBS peptide binds across the top surface of the β-propeller, forming an extensive interface (17). Mutations in either protein that disrupt the interface cause checkpoint deficiency and chromosome instability in yeast and human cells (17, 18). Bub3-bound BubR1 in turn can interact with Cdc20 in two fashions; on one hand, at unattached kinetochores, and on the other, cytoplasmically, resulting in the production of the mitotic checkpoint inhibitor (18).

$Bub3^{-/-}$ mice accumulate mitotic errors and do not survive beyond days 6.5–7.5 post coitus (5). Haplo-insufficient $Bub3^{+/-}$ mice exhibit increased chromosome instability, which results in a predisposition to carcinogen-induced lung tumors but does not result in an increased predisposition to spontaneous cancer development (6, 19–21).

In this study we evaluated the role of the human Bub3·BubR1 interaction for cancer cell growth and identified the specific protein interface that needs to be inhibited to abrogate the spindle assembly checkpoint function of Bub3. We show that tumor cells are more sensitive toward Bub3 depletion by shRNA than non-transformed cells. Single point mutations of conserved residues abolish the BubR1 binding to Bub3 in cells. Next we characterized the interaction of human Bub3 and BubR1. In the absence of detailed structural information, we generated a homology model based on the well studied yeast Bub3·Mad3 complexes (17) and validated the model using a panel of comple-

* All authors were Bayer Healthcare employees at the time the studies were conducted.

[1] To whom correspondence may be addressed. E-mail: florian.prinz@bayer.com.

[2] To whom correspondence may be addressed. E-mail: amaury.fernandez@bayer.com.

[3] The abbreviations used are: SAC, spindle assembly checkpoint; GLEBS, Gle2 binding sequence; MCC, mitotic checkpoint complex; IP, immunoprecipitation; SPR, surface plasmon resonance; Ni-NTA, nickel-nitrilotriacetic acid; FAM, fluorescein; TR-FRET, time-resolved FRET; ITC, isothermal titration calorimetry; TSA, thermal shift assay.

mentary biophysical and biochemical methods. Altogether, our data show that the Bub3 BubR1-GLEBS interaction is high affinity, long lasting, and enthalpy-driven, with a minimal 33-amino acid GLEBS peptide playing an essential role for the binding. Surprisingly, we found that the previously reported electrostatic interactions between the BubR1 GLEBS and Bub3 were not sufficient to ensure the stability of Bub3·BubR1 complexes, but the adjacent N- and C-terminal residues contribute synergistically to the observed high affinity and long half-life. Finally, we show that blocking the funnel of Bub3 is sufficient to abrogate the SAC, which could be therapeutically exploited to selectively target cancer cells.

Experimental Procedures

Cell Culture—Cell lines were obtained from different providers: HeLa, PC-3, and MCF-7 from the German Collection of Microorganisms and Cell Cultures (DSMZ, Germany); U2-OS, Hs68, MDA-MB-231, and MCF 10A cells from the ATCC; primary human fibroblasts from Provitro. Primary fibroblasts were grown in Earle's MEM (PAA) supplemented with L-glutamine (Biochrom) and 10% fetal calf serum (PAA). HeLa, MDA-MB-231, and MCF 10A cells were grown in DMEM/Ham's F-12 medium (Biochrom) supplemented with L-glutamine (Biochrom) and 10% fetal calf serum (PAA). PC-3 and U2-OS cells were cultured in RPMI 1640 medium supplemented with L-glutamine (Biochrom) and 10% fetal calf serum (PAA). Hs68 cells were maintained in DMEM supplemented with L-glutamine (Biochrom) and 10% fetal calf serum (PAA). MCF7 cells were grown in RPMI 1640 (Biochrom) supplemented with L-glutamine (Biochrom), 10 μg/ml bovine insulin (Sigma), 1×10^{-10} M estrogen (Sigma) and 10% FCS (PAA). Cell line identity was confirmed by STR DNA typing at DSMZ.

Cloning and Transfections—For siRNA transfections, cells were plated at 150,000 cells per well on 6-well plates in 2 ml of their respective media. After 24 h they were transfected with DharmaFECT 2 transfection reagent (Dharmacon) according to the manufacturer. Target siRNA SmartPool pools (Dharmacon) and control Dharmacon siGenome Non-Targeting #2 were used.

For overexpression of Bub3 and BubR1 fragments, the respective sequences were synthesized (Gene Art, Life Technologies) and cloned into pcDNA3.1 expression vectors. Plasmid purification was carried out using Qiagen Midi plasmid preparation kits (Qiagen, Hilden, Germany). Transfections were carried out in six-well plates using Amaxa electroporation (Life Technologies) for U2-OS and Lipofectamine 2000 (Life Technologies) according to the manufacturer's protocols. The following reference sequences were used for determination of the respective open reading frames: Bub3, gene ID 9184, NM_004725; BubR1 (Bub1B), gene ID 701, NM_001211.

For the generation of stable shBub3 clones, preselected shRNAs were cloned into the lentiviral pGT396-Puro vectors. The shRNA sequences of the forward oligonucleotides were as follows: sh_Control, 5′-TTCTCCGAACGTGTCACGTTTCAAGAGAACGTGACACGTTCGGAGAA-3′; sh_Control1, 5′-TAGCGACTAAACACATCAATTCAAGAGATTGATGTGTTTAGTCGCTA-3′; shBub3#828, 5′-GCAGATTTACCCAGTCAATGCTTCAAGAGAGCATTGACTGGGTAAATCTGC-3′; shBub3#889, 5′-GGTTCTGATGGCTTTGTAAATTTCAAGAGAATTTACAAAGCCATCAGAACC-3′; shBub3#965, 5′-GCATCGCATCACTTGCCTTCATTCAAGAGATGAAGGCAAGTGATGCGATGC-3′. Cells were transduced with a titer of 2 μg/ml p24. Selection was performed in the presence of 1 μg/ml puromycin (Sigma). When colonies were clearly visible, cells were fixed with 1% glutaraldehyde (Sigma) for 30 min at room temperature. Colonies were made visible by crystal violet staining (Sigma).

Lentiviruses were produced by co-transfecting the respective pGT396-Puro construct with lentiviral Packaging Mix (Invitrogen) into HEK-293FT cells (Invitrogen). Viral supernatants were concentrated by ultracentrifugation.

Quantitative Real-time PCR—For quantitative real-time PCR, RNA was extracted using the RNeasy Kit (Qiagen). For quantitative real-time-PCR, 500 ng of RNA were reverse-transcribed using RevertAid M-MuL Reverse Transcriptase (Life Technologies) according to the manufacturer's protocol. Subsequently, each cDNA sample was amplified in triplicate using TaqMan expression assays (Life Technologies). Hydroxymethylbilane synthase was used as endogenous control, and expression levels were calculated with the ΔΔCt method (22). The following Taqman assays were used: HS 00190920_m1 for Bub3 and HS 00609297_m1 for hydroxymethylbilane synthase (Applied Biosystems).

Proliferation and Apoptosis—For proliferation assays, cells were fixed by the addition of 11% glutaraldehyde (Sigma) and stained with 0.1% crystal violet (Sigma). Optical densities were read after dissolution of the dye in 0.1% acetic acid (Merck) at 595 nm. Apoptosis was determined using the Cell Death Detection ELISAPLUS (Roche Applied Science) according to the manufacturer's protocol, and optical densities were measured at 405 nm with reference wave length of 490 nm. Both assays were measured in an Infinite M200 Plate Reader, TECAN. The apoptotic index (apoptosis, normalized to cell number) was calculated by normalizing measured apoptosis (by Cell Death ELISA) to crystal violet signals.

Antibodies—Antibodies used for Western blotting were purchased from Sigma (anti-V5), BD Biosciences (Bub3, BubR1, cyclin B1, Hsp90), Millipore (MPM-2), and LifeSpan Biosciences (CDC20). For immunofluorescence we used anti-V5 (Abcam), anti-PH3 (Millipore), anti-rabbit-Dyelight488 (Vector Laboratories, Burlingame, CA), and Cy3 anti mouse (Jackson ImmunoResearch Laboratories, West Grove, PA). Immunoprecipitation was done with anti-V5 monoclonal mouse IgG (Sigma).

Immunoprecipitation and Immunoblotting—Where appropriate, cells were synchronized by the addition of nocodazole (Sigma) at a final concentration of 100 ng/ml for 16 h before lysis. For immunoblotting analysis, cells were harvested by scraping and lysed in radioimmune precipitation assay buffer (50 mM Tris, pH 7.5, 150 mM NaCl, 2 mM EDTA, 1% Triton X-100, 0.5% sodium deoxycholate, 0.1% SDS).

For immunoprecipitation experiments, cells were harvested by scraping and resuspended in IP lysis buffer (20 mM Tris, pH 7.6, 150 mM NaCl, 2 mM EDTA, 2 mM EGTA, 1% Nonidet P-40, 50 mM NaF, 10% glycerol with Protease Inhibitor Mixture (Roche Applied Science) and Phosphatase Inhibitor Cocktails I

and II (Sigma)). 1200 μg of protein were precipitated with anti-V5 monoclonal mouse IgG (5 μg antibody per 1000 μg of protein) and 10 μl of protein G-Sepharose (Sigma).

All samples were boiled in NuPAGE LDS sample buffer (Invitrogen) and separated and blotted using the NuPage and iBlot systems (Invitrogen). Detection was carried out using the ECL plus system (Amersham Biosciences).

Immunofluorescence—Lentivirus-transduced cells were grown on coverslips fixed for 15 min in 3.7% paraformaldehyde solution, permeabilized for 5 min with 0.5% Triton TX-100, and blocked for 60 min with 10% goat serum in PBS (blocking solution). Primary and simultaneous secondary antibody/Hoechst 33342 (1 μg/ml, Life Technologies) staining was each done for 60 min in blocking solution. Cells were analyzed under a Zeiss Axiovert 200M fluorescence microscope.

Proteins and Peptides—cDNA sequences of all proteins described below were synthesized (Gene Art, Life Technologies) and inserted into expression vectors using traditional cloning methods. The BubR1-GLEBS domain ($BubR1^{364-484}$) and the double mutant E409K/E413K ($BubR1^{364-484(E409K/E413K)}$) were cloned into pET16b and modified pET22b vectors (the GST tag from pGEX-KT was integrated into NdeI/SmaI site) for the overexpression of His- or GST-tag fusion proteins in *Escherichia coli*. Full-length Bub3 and BubR1 were cloned into a modified pVL 1392 vector for baculovirus generation and overexpression as N-terminal His- or GST-tagged fusion proteins in insect cells. All plasmids contained a PreScission protease cleavage site (LEVLFQGP) between the tag and the protein of interest.

BubR1 GLEBS variants were recombinantly expressed in the *E. coli* BL21DE3 strain. Cells were cultured in Circle Grow® medium at 37 °C, and expression was induced with 1 mM isopropyl 1-thio-β-D-galactopyranoside at $A_{600\,nm} \sim 1.0$. Upon 24 h of further culture at 17 °C, cells were harvested and stored at −20 °C. For baculovirus expression of full-length Bub3 and BubR1, SF9 cells (2×10^6 cells/ml) were infected with a multiplicity of infection 1, cultured in Grace's Medium (Invitrogen) with 5% FCS, and harvested after 72 h. Cell pellets were stored at −80 °C.

E. coli cell pellets were resuspended in buffer A^+ (50 mM Tris-HCl, pH 8.0, 250 mM NaCl, 10% glycerin, 5 mM DTT, with EDTA complete (Roche Applied Science)) and mechanically lysed using a Microfluidizer. Insect cells were lysed by adding 0.4% Nonidet P-40 to buffer A^+. Lysates were centrifuged at 100,000 × *g* for 1 h, and clear supernatants were loaded on a 5-ml His-Trap column or 5-ml GST-Trap column (both from GE Healthcare). Columns were washed with buffer A^+ and high salt buffer A^+ (500 mM NaCl) until the UV 280-nm baseline reached a stable level. In the case of His purification, 50 mM imidazole was added to the high salt buffer. Proteins were eluted by step elution using buffer A^+ supplemented with 400 mM imidazole or 30 mM reduced GSH, respectively. Eluates were dialyzed in buffer A^+ and further purified via size exclusion chromatography (Superdex 200 (GE Healthcare)) in the same buffer. Protein cleavage with PreScission was carried out overnight at 4 °C using 1 unit of protease per 0.1 mg of fusion protein followed by affinity and size exclusion re-chromatography. Purity and integrity of the purified proteins were controlled with SDS-PAGE and LC-MS analysis.

Human BubR1 GLEBS peptides were synthesized at Biosyntan using standard peptide chemistry methods. The C terminus was in its amide form unless it was used for the attachment of labels. Cysteine residues were replaced by norvaline in fluorescein (FAM)-labeled peptides to avoid FAM-induced oxidation and cysteine dimerization at neutral pH. Peptide sequences are available upon request.

Time-resolved Fluorescence Energy Transfer (TR-FRET)—TR-FRET measurements were carried out at room temperature in black 384-well low volume plates (Greiner) in a total volume of 5 μl. Each interaction was analyzed in at least two independent experiments with three or more replicates. Bub3 was diluted in 20 mM Tris/HCl, pH 8.0, supplemented with 250 mM NaCl and 5 mM DTT (buffer A) and added to the assay mix at final concentrations of 1 nM (His-Bub3) or 2.5 nM (GST-Bub3). BubR1 variants and TR-FRET labels were co-diluted in 50 mM Hepes, pH 7.5, supplemented with 0.01% BSA and 0.005% Triton X-100 (buffer B). For binding saturation experiments serial dilutions of the BubR1 variants were used at the indicated final concentrations. For competition experiments the concentrations of labeled BubR1 were fixed at 2.5 or 5.0 nM, and a serial dilution (in buffer B) of the unlabeled competitor was added to the assay at the indicated concentrations. TR-FRET detection reagents (all from Cisbio) were chosen depending on the tags present in the interacting proteins. Their final concentration in the assays was the same as the molecules to be labeled. In experiments involving His-Bub3 and GST-tagged BubR1 variants, Eu^{3+} cryptate/anti-His- and XL665/anti-GST antibody conjugates were, respectively, used as fluorescence donor and acceptor molecules. For assays with biotinylated BubR1 peptides, XLent-streptavidin was the acceptor molecule. Whenever the BubR1 GLEBS peptides were labeled with FAM as acceptor molecule, Tb^{3+} cryptate/anti-His- or anti-GST antibody conjugates were used as donor labels for Bub3. For binding saturation experiments, 2.5 μl of Bub3 and 2.5 μl of BubR1 variants with the corresponding detection reagents were mixed and incubated for 60 min before measuring the fluorescence signals. For competition assays 2 μl of Bub3 were preincubated 30 min with 1 μl (unlabeled) of competitor BubR1 variants before the addition of 2 μl of the labeled BubR1 tracers and further incubation (at room temperature) for 120 min. TR-FRET signals were acquired using a RUBYstar microtiter plate reader (BMG). The fluorescence donor was excited at a wavelength of 337 nm. For assays involving XL665 and XLent the acceptor (A)- and donor (B)-channel filters were set to 665 and 620 nm, respectively, whereas for experiments using FAM the A- and B-channel filters were set to 520 nm and 490 nm, respectively.

HTRF® ratio values were processed and analyzed using GraphPad Prism (version 6.00 for Windows). Blank-subtracted data from binding saturation and competition experiments were, respectively, fitted to the "one-site steady state" model assuming mass action binding at equilibrium with a small fraction of ligand bound and the "one-site competitive binding (fit K_i)" model based on the Cheng-Prusoff equation (23).

Surface Plasmon Resonance (SPR)—SPR interaction analyses were performed at room temperature on Biacore 2000 and T100 instruments (GE Healthcare). All assays involving immobilized Bub3 were conducted on Ni-NTA sensor chips using

0.01 M HEPES, pH 7.4, 0.15 M NaCl, 0.005% v/v Surfactant P20 (HBS-P+) as the capture/running buffer (all from GE Healthcare) at a flow rate of 5 μl/min. The ligand (50 nM His-Bub3 in HBS-P+) was captured during 180 s on the activated surface (see below) followed by a 60-s waiting time to allow baseline stabilization before each analyte injection cycle. Analytes (BubR1 GLEBS variants) were injected for 150 s, and dissociation in running buffer of the Bub3·BubR1 complexes was monitored for 450 s followed by the surface regeneration step described below. Seven increasing concentrations (the highest depending on the affinity) of the BubR1 variants (diluted 2-fold) and a buffer blank were analyzed in three or more independent experiments. Surface conditioning was performed as described elsewhere (24). Briefly, activation/regeneration was achieved with subsequent injections (160 s and 60 s, respectively) of 500 mM EDTA (in HBS-P+ buffer adjusted to pH 8.3) and 1 M $NiCl_2$ (in HBS-P+, with pH readjusted to 7.4).

In a different experiment setup, 10 μM biotinylated BubR1 GLEBS peptides were captured on SA-coated chips (GE Healthcare) following standard protocols (25), and the surface was flooded with a 2-fold dilution of GST-Bub3 (0–100 nM, 6-point) using a single cycle kinetics protocol (26) with 120-s association and 600-s dissociation times.

To obtain the kinetic and affinity parameters, double-referenced kinetic and steady-state binding responses, respectively, were fitted to a Langmuir 1:1 interaction model (Biacore™ Assay Handbook) and to a one-site specific binding model (see below) using the BiaEval™ analysis software (GE Healthcare). Surface activities were calculated as described elsewhere (Biacore™ Assay Handbook).

Isothermal Titration Calorimetry (ITC)—ITC was performed at 25 °C in an ITC_{200} microcalorimeter (MicroCal, Inc., Northampton, MA). 7–10 μM concentrations of various BubR1 peptides were titrated with 70–170 μM GST-Bub3 or cleaved Bub3 in 20 mM Tris/HCl, pH 8.0, 250 mM NaCl, 10% glycerol, 1 mM tris(2-carboxyethyl)phosphine using injections of 2 μl within 4 s at 120-s intervals and 1000 rpm stirring speed. Reference Power was set to 6 μcal/s and the filter period to 2 s. Data were collected on high feedback mode. Analysis was performed with a single binding site model in the Origin MicroCal analysis software (version 7 SR4, MicroCal, Inc.). No more than 10% of data were excluded from analysis.

Thermal Shift Assay (TSA)—TSAs (a.k.a. differential scanning fluorometry) were performed in a 7500 Real Time PCR System (Applied Biosystems). Interactions were studied in 96-well Optical Reaction Plates (Applied Biosystems) in a final volume of 10 μl per well. Test samples contained 0.5 μg of His-Bub3, 5× Sypro Orange (Molecular Probes) and synthetic BubR1 GLEBS peptides at 0, 1.25, 3.70, or 12.50 μM (molar ratios of 1:0, 1:1, 1:3, and 1:10) in 50 mM Hepes, pH 7.5, 50 mM KCl, and 0.005% Triton X-100. Negative control experiments containing all reaction components except Bub3 were included. Before the measurement the plates were sealed with MicroAmp™ Optical Adhesive Film (Applied Biosystems). Protein melting curves were recorded by increasing the temperature from 20 °C to 90 °C at a ramp rate of 1% (1 °C/min), whereas fluorescence signals were acquired simultaneously using the filter recommended by the instrument manufacturer.

Raw temperature-dependent fluorescence signals corresponding to the thermal denaturation of Bub3 were processed with a Microsoft Excel macro that used a first-derivative algorithm to calculate the temperature at which the upward slope of the fluorescence *versus* temperature curve is the steepest (T_m). Thermal stabilization (ΔT_m) was defined as the difference between the Bub3 T_m in the presence and absence of the BubR1 GLEBS interacting peptides. The data shown under "Results" correspond to the average of two independent experiments, each with three replicates.

Homology Model of Human BUB3—Primary-sequence comparisons between the *Homo sapiens* Bub3 (O43684) sequence and the PDB database identified three template structures (PDB codes 2I3T, 2I3S, and 4BL0) suitable for homology modeling of the *H. sapiens*. Bub3 WD40 domain. Pairwise alignments between each template structure and the target sequence were determined. 100 three-dimensional models of the WD40 domain were then generated from each template, and the model with the best probability density function total was chosen for further analysis. The stereo-chemical quality of each model was confirmed. All calculations were carried out using the Discovery Studio Suite 4.1 software suite (Accelrys).

Results

Human Bub3 Knockdown Abrogates the Spindle Assembly Checkpoint, Promotes Apoptosis, and Inhibits the Proliferation of Tumor Cells—In our first experiments we wanted to analyze the effects of Bub3 genetic knockdown in several human tumor and non-transformed cell lines. The aim of these studies was to test whether the mitotic failures with severe chromosome segregation defects and cell death previously observed in other organisms or individual cell lines (4–7, 18, 27) could be translated to a broader panel of clinically relevant human cancer cell lines. Furthermore, we wanted to know if this phenomenon applies to all cell types equally or whether there might be a "therapeutic window" between cancer and non-transformed cells.

Several tumor cell lines (HeLa, PC3, MCF-7, U2-OS, MDA-MB-231) and non-transformed cells (primary human fibroblasts, Hs68, MCF 10A) were transduced with lentiviruses encoding shRNAs targeting Bub3, and changes in nuclear morphology, proliferation rates, and apoptosis induction were characterized. As exemplified by the U2-OS line, tumor cells showed a large increase in the number of micronuclei upon Bub3 silencing (Fig. 1*A*, *upper panel*). This phenotype points to premature entry of these cells into anaphase with consequent mitotic failures and chromosome mis-segregations. In contrast, no changes were observed in the nuclear morphology of non-transformed Hs68 human fibroblasts (Fig. 1*A*, *lower panel*). Alterations in nuclear morphology were not obvious even after long term knockdown (not shown). We also observed that depletion of Bub3, but not the structurally related Rae1, resulted in abrogation of the spindle assembly checkpoint, as indicated by reduced MPM-2 phospho-antigen and cyclin B1 levels in nocodazole-treated cells as compared with untreated control cells (Fig. 1*B*). These findings establish and validate the link between the nuclear phenotype induced by Bub3 depletion and a malfunctioning SAC for a variety of human cancer types.

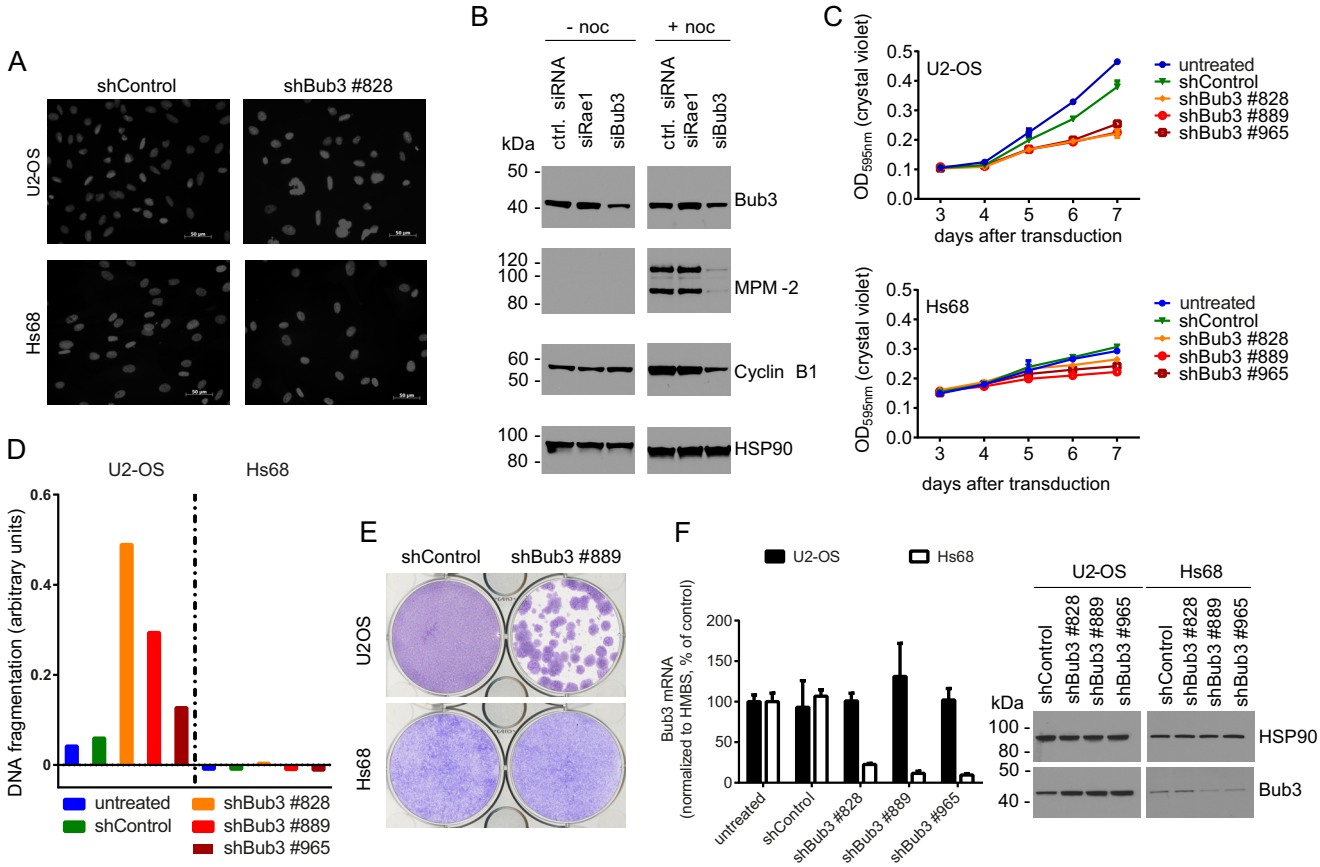

FIGURE 1. **Effects of Bub3 knockdown on SAC signaling, apoptosis, and cancer cell proliferation.** *A*, nuclear morphology of U2-OS (*top*) and Hs68 (*bottom*) cells after 6 days of Bub3 silencing. *B*, Western blots of Bub3 and mitotic markers MPM-2 and cyclin B1 in cell lysates from siRNA-transfected HeLa cells 48 h after transfection with (+) and without (−) nocodazole (*noc*) treatment to induce mitotic arrest. HSP90 was used as a loading control. 20 μg of total protein were loaded on each lane. Molecular mass markers are indicated on the *left hand side of the blots*. *C*, proliferation curves of U2-OS (*top*) and Hs68 (*bottom*) cells after shRNA-mediated knockdown of Bub3. Representative growth curve of three independent experiments; *error bars*, mean ± S.D. *D*, apoptotic index (*y* axis) after 6-days of shRNA-mediated knockdown of Bub3 in U2-OS and Hs68 cells. Measured DNA fragmentation was normalized to cell number from C. *E*, outgrowth of U2-OS tumor cells and Hs68 cells after lentiviral transduction with shBub3 or control shRNA. Cells were fixed and stained with crystal violet 3 weeks after transduction and puromycin selection. *F*, *left*, quantitative RT-PCR (Taqman) analysis of Bub3 expression in samples after 3 weeks of long term silencing as shown in *E*. Hydroxymethylbilane synthase was used as endogenous control. For each cell line Bub3 expression levels were normalized to Bub3 expression levels in untreated growing cultures. *Right*, Western blot of Bub3 protein levels in cell lysates from a parallel sample after 3 weeks of Bub3 knockdown with HSP90 used as a loading control. 15 μg total protein were loaded on each lane. Molecular mass markers are indicated on the *left hand side of the blots*.

Because aneuploid tumor cells are highly dependent on SAC function (for review, see Refs. 28 and 29) and, therefore, could be more susceptible to SAC abrogation than non-transformed cells, our findings encouraged us to evaluate the effect of Bub3 knockdown on apoptosis induction and proliferation in U2-OS and Hs68 cells. A significant anti-proliferative effect on U2-OS tumor cells was observed after Bub3 depletion, whereas growth rates of non-transformed Hs68 cells were not significantly affected (Fig. 1*C*). Accordingly, a significant apoptosis induction was measured in U2-OS cells upon Bub3 depletion, whereas non-transformed Hs68 cells remained unaffected (Fig. 1*D*). Similar effects were observed in HeLa, MCF-7, or MDA-MB-231 tumor cells and primary human fibroblasts or MCF10A non-transformed cells, respectively (data not shown).

To exclude artifacts resulting from different population doubling times in tumor and non-transformed cells, we conducted long term knockdown experiments. Cells were transduced with lentiviruses encoding both shRNAs and antibiotic resistance. After 3 weeks of selection, surviving cells were visualized with crystal violet and analyzed for remaining Bub3 protein. In U2-OS tumor cells the long term Bub3 knockdown resulted in the outgrowth of individual clones. In contrast Hs68 cells produced a homogenous layer of cells (Fig. 1*E*).

Unexpectedly, analysis of both Bub3 mRNA and protein levels after long term silencing showed that strong Bub3 mRNA and protein depletion had been only achieved in surviving Hs68 but not U2-OS cells. Hs68 cells endured selection with as little as 20% residual Bub3 mRNA and protein levels, whereas outliving U2-OS cells showed unchanged Bub3 protein levels (Fig. 1*F*). Of note, short term silencing of Bub3 resulted in a similarly strong mRNA and protein depletion in both cell lines (not shown), indicating that in the long term experiments those U2-OS cells with a strong Bub3 knockdown are more prone to die, whereas those with a weak knockdown are likely to form the surviving clones. Taken together, our data show that tumor cells are more sensitive toward Bub3 depletion than non-transformed cells, suggesting that targeting human Bub3 interactions in the mitotic checkpoint complex could be a valid therapeutic strategy to tackle proliferative disorders.

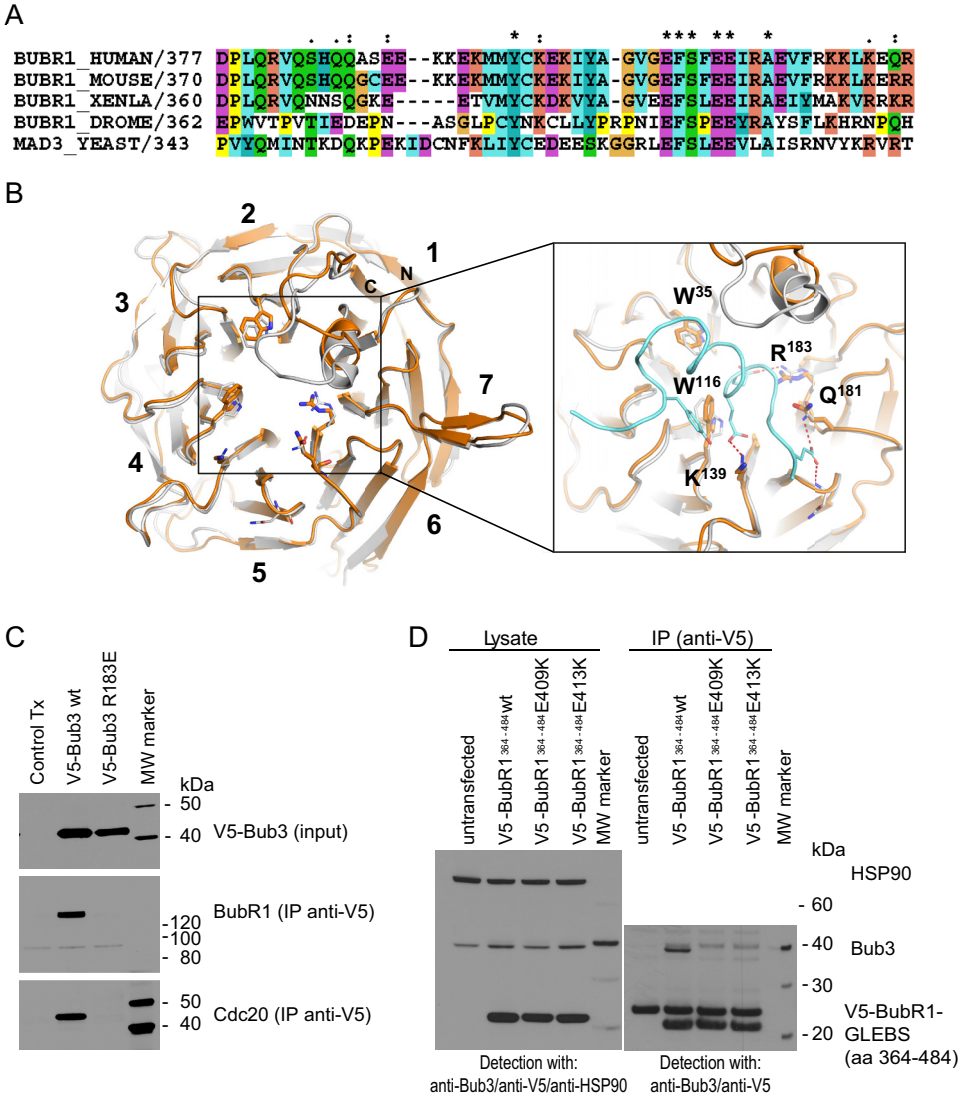

FIGURE 2. **Characterization of human Bub3·BubR1 GLEBS domain interactions.** *A*, sequence alignment showing conservation of the BubR1 GLEBS peptide from yeast to man. Identical residues over all species marked with (*), (:) and (.) and mark descending degrees of conservation (Ref. 33; ClustalX2 default, accessions from Uniprot). *B*, homology model of human Bub3 (*gold*) based on the structure of yeast Bub3 (*gray*) bound to Mad3 (*blue*). The close-up shows the conserved interactions at the funnel of the Bub3 WD40-fold. *C*, Western blot analysis after IP of ectopically expressed, V5-tagged Bub3 (WT and R183E mutated) variants. Detection was carried out with anti-V5, anti-Cdc20, and anti-BubR1 antibodies. For input samples, 15 μg of total protein were loaded per lane. For immunoprecipitation, 1200 μg of total protein were used, and the complete precipitate was loaded onto the gel. Molecular mass markers are shown on the *right hand side of the blots*. *D*, Western blot analysis after IP of ectopically expressed, V5-tagged BubR1 GLEBS domain variants. Detection was carried out with anti-Bub3 and anti-V5 antibodies. For lysate samples, Hsp90 was used as a loading control, and 15 μg of total protein were loaded per lane. The *upper band* in the IP section of the V5-GLEBS blot represents the light chain of the anti-V5 IP antibody. 1200 μg of total protein were used per immunoprecipitation, and the complete precipitate was loaded onto the gel. Molecular mass markers are shown on the *right hand side of the blots*.

Specific Interactions of Bub3 with Bub1 and BubR1 Are Essential for Mitotic Checkpoint Complex Integrity in Human Cells—In the next step we focused on the interspecies conservation of Bub3 interactions at the MCC. X-ray crystal structures of yeast Bub3 in complex with GLEBS motif peptides from either Mad3/BubR1 or Bub1 have identified essential interface interactions, including, for example, salt bridges between *Saccharomyces cerevisiae* Bub3$^{Arg\text{-}197}$ and Mad3$^{Glu\text{-}337/Glu\text{-}382}$ or Bub1$^{Glu\text{-}233/Glu\text{-}337}$ (17). Sequence comparison (Fig. 2*A* and Ref. 17) indicate that these key residues are conserved at a primary sequence level. To assess whether these interactions are also conserved at a tertiary structural level within the human Bub3 protein, we calculated a homology model of the *H. sapiens* Bub3 WD40 protein domain (Fig. 2*B*). The model predicts that human Bub3 adopts a canonical seven-bladed β-propeller fold, whereby seven sets of four-stranded β-sheets are arranged around a central pore. At the predicted GLEBS binding site of human Bub3, both the architecture and sequence identity is highly conserved with the yeast Bub3 protein. Specifically, this suggests that contacts essential for the yeast Bub3/GLEBS interaction are also critical for the human Bub3/GLEBS interaction.

To test this hypothesis we used our homology model to guide the design of a human Bub3^{R183E} mutant. The equivalent yeast mutation (*S. cerevisiae* Bub3^{R197E}) results in disruption of the Bub3·Mad3/BubR1 complexes (17). V5-tagged forms of both human wild type and R183E Bub3 proteins were expressed in HeLa cells. Immunoprecipitation of Bub3 followed by Western blotting demonstrated the presence of endogenous BubR1 and

Cdc20 in the IP eluates of cells transfected with the wild type Bub3 but not in cells expressing the R183E mutant (Fig. 2*C*). These results validated the Bub3 homology model and provided further explanation for the effects observed in the Bub3 knockdown studies, suggesting that specific interactions of Bub3 with the Bub1/BubR1 GLEBS domains are essential to keep the integrity of the MCC in human cells.

Subsequently we ectopically expressed and immunoprecipitated V5-tagged human BubR1 GLEBS domain (amino acids 364–484) from HeLa cells. In agreement with a recent report (18), we were able to detect endogenous Bub3 in the immunoprecipitate. However, when the BubR1 GLEBS domain mutants E409K or E413K were expressed with the same efficiency and pulled down, Bub3 was absent from the immunoprecipitates (Fig. 2*D*). From these studies we concluded that specific binding of BubR1 to Bub3 is required for the stability of the mitotic checkpoint complex and, consequently, the spindle assembly checkpoint and decided to focus further on the characterization of this interaction at the molecular level.

The BubR1-GLEBS Domain Builds Tight, Long Lasting, and Enthalpy-driven 1:1 Complexes with Bub3—The results from the experiments described above demonstrated the relevance and specificity of the interaction between Bub3 and the BubR1 GLEBS domain in cells. In the following step we quantified the affinity of this binding event, a feature that to our knowledge has not been yet described for the human proteins. To this end we expressed and purified recombinant human full-length Bub3 and a BubR1 GLEBS domain construct comprising the same amino acid sequence used for the immunoprecipitation studies (BubR1$^{364-484}$). We also produced a double mutant of the previous construct (BubR1$^{364-484(E409K/E413K)}$) based on the results obtained in cells with the respective single mutants. Proteins were expressed in-frame with His or GST tags to enable affinity chromatography purification and labeling with fluorescent tags for interaction studies. We then characterized the interaction with three orthogonal and complementary biochemical and biophysical methods (TR-FRET, SPR, and ITC), aiming to generate as much information as possible about this binding event.

In the first experiments we labeled Bub3 with a TR-FRET donor and titrated both BubR1$^{364-484}$ and BubR1$^{364-484(E409K/E413K)}$ labeled with the corresponding fluorescence acceptor (Fig. 3*A*). We measured specific binding of the wild type with a K_D of 2.12 ± 0.29 nM, whereas, consistent with the results shown in the previous section, the introduction of the double mutation completely abolished binding. The specificity and high affinity of the binding was again demonstrated in a competition assay in which labeled BubR1$^{364-484}$ was completely displaced by increasing concentrations of the untagged protein with a K_i of 0.67 ± 0.11 nM (Fig. 3*B*). Likewise, the formation of Bub3 complexes with BubR1$^{364-484}$ was inhibited with comparable efficiency (K_i = 2.48 ± 0.24 nM) by an untagged BubR1$^{392-425}$ synthetic peptide. This result prompted us to test this BubR1$^{392-425}$ peptide with N- or C-terminal biotin tags and SA-Lent labels in saturation binding titrations (not shown), which yielded similar K_D values as the BubR1$^{364-484}$ protein (Table 1).

We next sought to confirm our TR-FRET observations with an alternative orthogonal "label-free" SPR assay. Upon injection of BubR1$^{364-484}$ onto immobilized Bub3, the resulting SPR sensorgrams show a concentration- and time-dependent response unit increase, which is characteristic of complex formation during the analyte injection phase (Fig. 3*C*). In the same experiment, BubR1 dissociation from Bub3 took place at a very slow rate, which is typical of a tight, long half-life interaction. Global fit of this traces to a Langmuir 1:1 mode delivered an association rate for the interaction (k_{on}) of $1.37 \times 10^5 \pm 3.2$ $M^{-1}\cdot s^{-1}$ and a dissociation rate (k_{off}) $<1.0 \times 10^{-5}$ s^{-1} ($t_{1/2} > 2$ h). To rule out the possibility that the high affinities measured with SPR were due to unspecific binding of the GST moiety not corrected by the standard double referencing (30) used, we tested untagged synthetic BubR1$^{392-425}$ and BubR1$^{392-425(E409K/E413K)}$ peptides under the same experimental conditions. In these experiments the double mutant peptide did not show measurable binding to Bub3 up to a concentrations of 25 μM (data not shown), whereas the results for the "wild type" BubR1$^{392-425}$ peptide were quite similar to those obtained with the 4-fold larger GLEBS peptide (see Fig. 5*A*, Table 1).

Further validation to our findings was provided by ITC. The titration of BubR1$^{392-425}$ with Bub3 (Fig. 3*D*, Table 1) demonstrated that the interaction between human BubR1 and Bub3 is stoichiometric (1:1) and enthalpy-driven. The ΔH of −17.8 ± 0.2 suggests a network of favorable enthalpic interaction, whereas the entropic contribution ($-T\Delta S$) of 7.7 kcal·mol^{-1} may reflect a loss in entropy due to *e.g.* a reduction of peptide's conformational freedom upon binding to Bub3. The affinity measured for the interaction (37 nM) was lower than the K_D detected with other methods. A possible explanation for this discrepancy could be that the ITC measurements were conducted at a higher ionic strength compared to the TR-FRET and SPR experiments. Indeed, TR-FRET ratios for a FAM-labeled peptide of the same sequence dropped slightly (1.6-fold) when tested at 30 nM in a buffer containing 250 mM NaCl, and the affinity of the BubR1$^{364-484}$-Bub3 interaction decreased in similar proportion in saturation binding experiments conducted at increasing ionic strengths, with a maximum K_D shift of 3-fold observed at 1.5 M NaCl (data not shown). These results do not fully explain the 10-fold gap for the ITC K_D; therefore, we cannot exclude a more complex binding mode (*e.g.* involving conformational changes), which may in turn result in additional thermodynamic phenomena reflected by the ITC measurements. This might be also one of the reasons underlying the different FRET efficiencies observed with various constructs and protein preparations in TR-FRET experiments. Taken together, our results demonstrate that the interaction between Bub3 and the BubR1 GLEBS motif is of high affinity, has a long half-life, and is thermodynamically characterized by a strong enthalpy component.

The Bub3 Binding Affinity of BubR1 GLEBS Is Modulated by Its N- and C-terminal Regions—Having shown that the GLEBS domain of human BubR1 interacts very tightly with human Bub3, we sought to characterize the relative contributions of different regions of this motif toward the overall binding affinity. Based on high levels of interspecies sequence conservation within the GLEBS domains (Fig. 2*A* and Ref. 17) and our homology model, we synthesized four partially overlapping BubR1

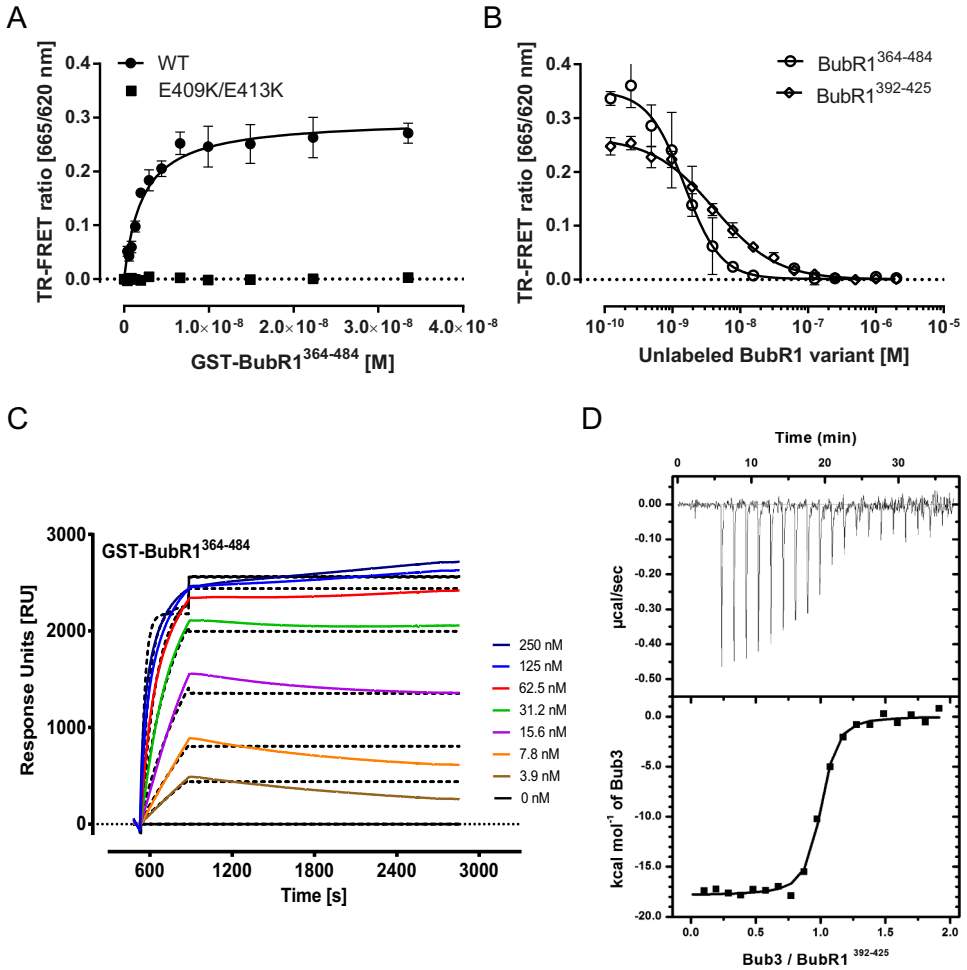

FIGURE 3. **Affinity, kinetics, and thermodynamics of human Bub3·BubR1 GLEBS domain interactions.** *A*, TR-FRET saturation binding curves corresponding to the titration of GST-BubR1 GLEBS domain amino acids 364–484 (*circles*) and the double mutant E409K/E413K (*squares*) at the concentrations indicated on 1 nM His-Bub3. Tagged proteins were labeled with an anti-GST-XL665 and anti-His Eu3+ cryptate antibody conjugates, respectively. Fitting of the data to a one-site specific binding model (*lines*) generated the K_d values shown in Table 1. *B*, TR-FRET inhibition curve resulting from the titration of untagged BubR1$^{364-484}$ (*circles*) or BubR1$^{392-425}$ (*squares*) at the concentrations indicated in a mixture of 2.5 nM GST-BubR1$^{364-484}$ and 1 nM His-Bub3 labeled as described above. Fitting of the data to a competitive binding model (*lines*) resulted in the K_i values shown in Table 1. *C*, SPR sensorgrams corresponding to the injections of increasing concentrations of GST-BubR1$^{364-484}$ on a Ni-NTA sensor chip coated with His-tagged Bub3. Analysis of the data with a Langmuir model (*dotted lines*) resulted in the kinetic and affinity parameters shown in Table 1. *D*, ITC titration of BubR1$^{392-425}$ on His-Bub3 at the concentrations indicated under "Experimental Procedures." Analysis of the data with a single site binding model (*lines*) delivered the thermodynamic and affinity data shown in Table 1.

peptides, BubR1$^{392-425}$, BubR1$^{400-425}$, BubR1$^{392-419,}$ and BubR1$^{400-419}$ (sequence numbering from *H. sapiens* BubR1, gene ID 701, see Fig. 2*A*) with and without N-terminal FAM labels (Fig. 4*A*) to allow us to compare and characterize the respective binding contributions and importance of three distinct regions of the GLEBs motif in TR-FRET binding and competition assays. The data shown in Fig. 4 and Table 1 revealed the effects of the mutations on the respective peptide affinities. Removing the N terminus of the GLEBS peptide resulted in a 600-fold affinity loss in the binding saturation assay (GST-Bub3 *versus* BubR1$^{400-425}$), whereas deleting the C terminus decreased the K_D by nearly 300-fold (GST-Bub3 *versus* BubR1$^{392-419}$). Deletion of both N and C termini (GST-Bub3 *versus* BubR1$^{400-419}$) had strong antagonistic effects on the affinity of the interaction, with a decrease in K_D of nearly 6000-fold (Fig. 4*B*). The overall results obtained from the titration of the labeled peptides were confirmed in homo- and heterogeneous competition experiments in which the interaction of the fluorescein-labeled BubR1$^{392-425}$ and Bub3 was outcompeted by the untagged BubR1 variants with K_i values similar to the K_D values previously calculated in saturation binding experiments (Fig. 4*C* and Table 1).

To rule out artifacts produced by the labeling of the peptides and Bub3 with fluorescent dyes, bulky affinity tags, and conjugated antibodies, we devised a differential scanning fluorometry assay to study the effects of the same peptides without label on the thermal unfolding of a Bub3 protein bearing only a hexahistidine tag (Fig. 4*D*). BubR1$^{392-425}$ binding to Bub3 results in a significant concentration-dependent thermal stabilization of the protein: ΔT_m shifts of 6, 13, and 16 °C were observed for Bub3:BubR1 molar ratios of 1:1, 1:3, and 1:10. We observed similar effects with the BubR1$^{392-419}$ protein, albeit more attenuated (0, 3, and 7 °C, respectively). For the peptides BubR1$^{400-425}$ and BubR1$^{400-419}$, no stabilization was observed.

Our findings combined with the results for the E409K/E413K mutant suggest that the contacts established by these amino acids are necessary, but not sufficient, for the establishment of

TABLE 1

Binding affinity, thermodynamic, and kinetic parameters for the interaction of BubR1 variant with full length Bub3

Italicized values indicate that the data were obtained in an heterogeneous competition assay using FAM-BubR1$^{392-425}$ as tracer.

Ligand	Method/Parameter														
	TR-FRET (binding)	TR-FRET (competition)	TSA	ITC				SPR							
	K_D	K_i	dT_m	K_D	ΔH	$-T\Delta S$	N	k_{on}	k_{off}	$K_{D\,kin}$	$K_{D\,eq}$	Surface activity
					kcal·mol^{-1}	*kcal·mol*$^{-1}$		$M^{-1}s^{-1}$	s^{-1}			
BubR1^{FL}	$1.19 \times 10^{-9} \pm 4.09 \times 10^{-10}$	*M*[a]	*K*[a]	*M*	/	/	/	/	/	*M*	*M*	*M*	%
BubR1$^{364-484}$	$2.12 \times 10^{-9} \pm 2.89 \times 10^{-10}$	$6.67 \times 10^{-10} \pm 1.11 \times 10^{-10}$	/	/	/	/	/	$1.37 \times 10^{5} \pm 3.2$	$<1.00 \times 10^{-5}$	/	/	/	/
BubR1$^{392-425}$	$4.38 \times 10^{-9} \pm 1.01 \times 10^{-9}$[d]	$1.02 \times 10^{-9} \pm 2.50 \times 10^{-10}$	16 ± 0.0	$3.70 \times 10^{-8} \pm 7.3 \times 10^{-9}$[f]	-17.8 ± 0.2[f]	7.7[f]	0.96 ± 0.007[f]	$1.00 \times 10^{6} \pm 1.22 \times 10^{3}$	$<8.78 \times 10^{-5} \pm 9.91 \times 10^{-11}$	/	$<1.39 \times 10^{-10}$	$<1.28 \times 10^{-8}$[c]	47.3
	$2.77 \times 10^{-9} \pm 4.51 \times 10^{-10}$[g]			$8.33 \times 10^{-8} \pm 8.7 \times 10^{-9}$	-18.9 ± 0.2	9.2	0.7 ± 0.005	/	/	/	$<6.95 \times 10^{-9}$	$<6.95 \times 10^{-9}$[c]	120.2 ± 10.1
	$1.17 \times 10^{-9} \pm 1.93 \times 10^{-10}$[e]			/	/		/	/	/	/	/	/	/
BubR1$^{400-425}$	$3.51 \times 10^{-7} \pm 1.19 \times 10^{-7}$	*1.10* $\times$ *10*$^{-7}$ *±* *3.29* $\times$ *10*$^{-8}$	7.0 ± 0.6	$3.86 \times 10^{-7} \pm 8.90 \times 10^{-8}$	-9.4 ± 0.4	0.6	0.8 ± 0.02	$5.89 \times 10^{5} \pm 1.21 \times 10^{2}$	$4.77 \times 10^{-2} \pm 1.72 \times 10^{-5}$	8.56×10^{-8}	1.32×10^{-7}	100.7 ± 27.4
BubR1$^{392-419}$	$1.20 \times 10^{-6} \pm 2.45 \times 10^{-7}$	*2.40* $\times$ *10*$^{-7}$ *±* *1.31* $\times$ *10*$^{-7}$	1.0 ± 0.0	$1.56 \times 10^{-7} \pm 3.86 \times 10^{-8}$	-15.8 ± 0.6	6.5	0.7 ± 0.02	$1.10 \times 10^{6} \pm 3.15$	$3.02 \times 10^{-3} \pm 1.52 \times 10^{-8}$	3.29×10^{-9}	$<1.59 \times 10^{-8}$[c]	103.9 ± 1.3
BubR1$^{400-419}$	$6.96 \times 10^{-6} \pm 9.57 \times 10^{-7}$	*3.36* $\times$ *10*$^{-6}$ *±* *1.16* $\times$ *10*$^{-6}$	-1.0 ± 0.6	$8.27 \times 10^{-7} \pm 2.12 \times 10^{-7}$	-2.7 ± 0.2	-5.6	1.0 ± 0.04	$>1.00 \times 10^{6}$	>1.00	_[b]	1.34×10^{-5}	71.9 ± 22.8
BubR1$^{392-425(E393A)}$	$4.46 \times 10^{-8} \pm 5.15 \times 10^{-9}$	*9.26* $\times$ *10*$^{-8}$ *±* *1.75* $\times$ *10*$^{-8}$	2.0 ± 0.0	/	/	/	/	$1.91 \times 10^{5} \pm 1.21 \times 10^{-2}$	$4.93 \times 10^{-4} \pm 3.16 \times 10^{-11}$	2.59×10^{-9}	$<4.12 \times 10^{-8}$[c]	132.2
BubR1$^{397-425}$	$5.31 \times 10^{-7} \pm 1.06 \times 10^{-7}$	*7.26* $\times$ *10*$^{-8}$ *±* *2.4* $\times$ *10*$^{-8}$	2.0 ± 0.6	/	/	/	/	$1.05 \times 10^{4} \pm 1.37 \times 10^{-3}$	$5.66 \times 10^{-4} \pm 7.68 \times 10^{-11}$	5.37×10^{-8}	$<3.91 \times 10^{-7}$[c]	162.4

[a] Not measured.
[b] Not calculated.
[c] Upper limit estimate.
[d] N-terminal biotin.
[e] N-terminal FAM.
[f] Untagged Bub3.
[g] C-terminal biotin.

tight Bub3·BubR1 complexes. In addition to the "core" region of the GLEBS peptide (amino acids 400–419), the N-terminal region (amino acids 392–400) with its Glu-394 salt bridge makes an important contribution to the binding, followed by the C-terminal part (amino acids 419–425). Interestingly, the point mutation E394K resulted only in a 10-fold decrease (K_D = 44.6 ± 5.15 nM, K_i = 92.6 ± 17.5 nM) of the binding affinity, suggesting that other contacts within this region are contributing to the binding energy. Along these lines, the binding of a BubR1$^{397-425}$ was 10-fold weaker than the E394K mutant and similar to the BubR1$^{400-425}$ peptide (data not shown).

Kinetics and Thermodynamics Components of Bub3 Binding by BubR1 GLEBS Mutants—The distinct contributions of the BubR1 GLEBS variants to the binding affinity motivated us to further characterize the molecular mechanism by which they recognize Bub3. To this end we performed a detailed analysis of the dynamics and energetics of the interactions using SPR and ITC.

Binding kinetics analysis of the interaction of BubR1 GLEBS variants with Bub3 (Fig. 5*A*, Table 1) revealed some differences in the equilibration dynamics (k_{on}). BubR1$^{392-425}$ and BubR1$^{392-419}$ associate faster than all peptides bearing deletions or point mutations in the N-terminal part. The only exception to this trend was the BubR1$^{400-419}$, which showed diffusion-controlled association rates. For the dissociation rates, major differences among the variants studied were observed. The N-terminal part of the GLEBS peptide has an important contribution to the long $t_{½}$ of the interaction, as its deletion (BubR1$^{400-425}$) results in a 500-fold decrease in k_{off} compared with BubR1$^{392-425}$. In contrast, the C-terminal deletion (BubR1$^{392-419}$) shows only a 30-fold decrease compared with BubR1$^{392-425}$. Surprisingly, the peptide core bearing Glu-409 and Glu-413 is not responsible for the slow dissociation kinetics; in fact, BubR1$^{400-419}$ was the only variant showing a transient binding to Bub3, and the kinetic parameters for this interaction could not be determined accurately by the Biacore instrument. Interestingly, the contribution of the N-terminal sequence to the long residence time does not seem to be mediated by interactions via Glu-394, as a BubR1$^{392-425(E394K)}$ mutant showed the second smallest k_{off} of all variants. Furthermore, a BubR1$^{397-425}$ peptide displayed the same k_{off} but, intriguingly, this variant displayed a 10-fold decrease in k_{on} and affinity compared with BubR1$^{392-425(E394K)}$. This suggests that 1) the residues surrounding Glu-394 play an important role in the association kinetics, and 2) the contacts established by the BubR1 residues Met-397, Tyr-398, and Cys-399 are extremely important for the long half-life of the interaction. All in all, these data show that the high affinity of the BubR1 GLBS fragment for Bub3 is kinetically driven by a very small k_{off}, which was estimated to be $<1 \times 10^{-5}$ s^{-1}.

From the thermodynamics perspective, BubR1$^{392-425}$ binding to Bub3 is, as discussed above, an enthalpy-driven event, and this is also the case for BubR1$^{392-419}$ and BubR1$^{400-425}$ (Fig. 5*B*, Table 1). Interestingly the entropic contribution of the C-terminally deleted peptide is similar to the one of the full-length peptide, whereas removing the N-terminal part results in a 10-fold drop in $-T\Delta S$, suggesting that binding of this region may be associated to conformational changes in Bub3. Again, BubR1$^{400-419}$ stands out for its different mode of action:

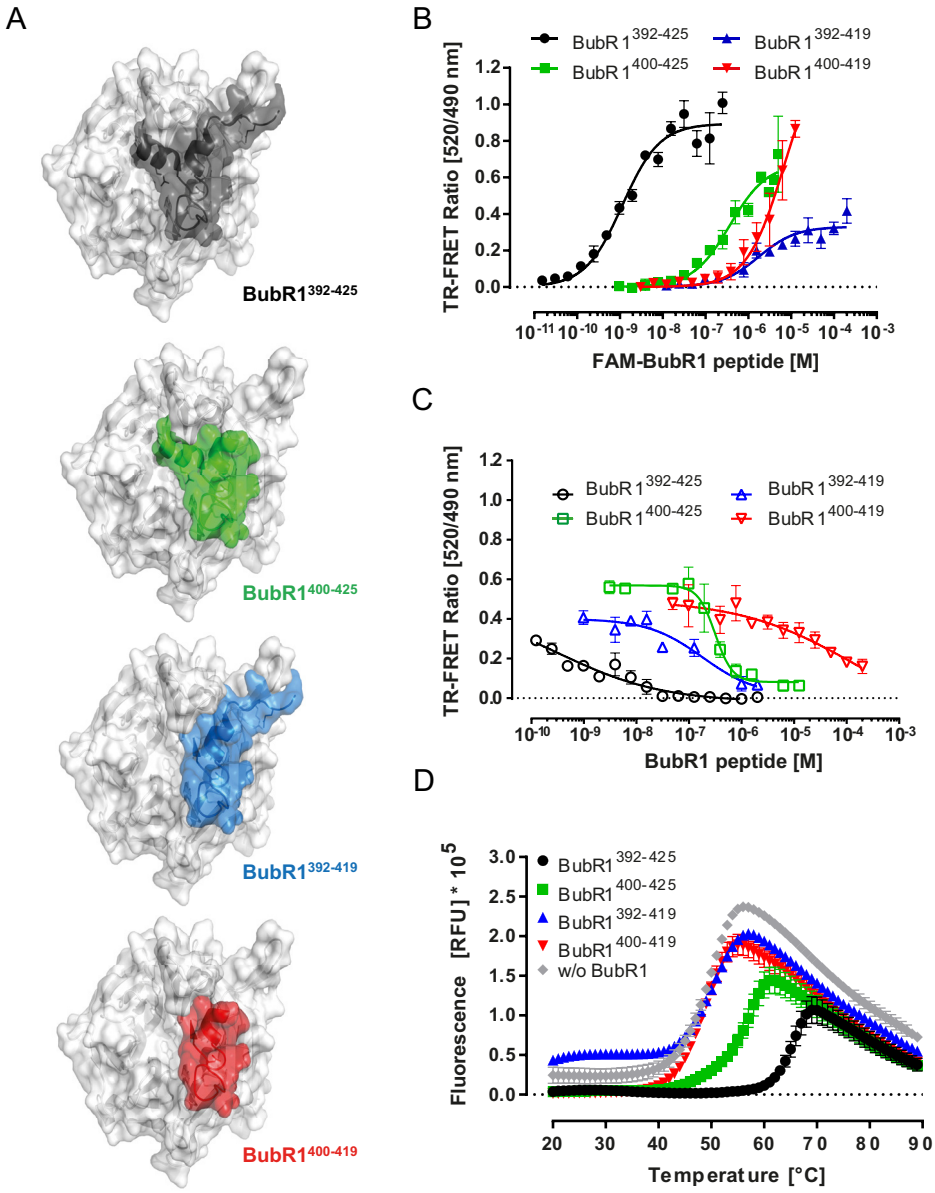

FIGURE 4. **Characterization of the structural determinants for the high affinity interaction between human Bub3 and BubR1 GLEBS motif.** *A*, tridimensional representation of the binding mode predicted for the BubR1 GLEBS variants studied. *B*, TR-FRET saturation binding curves corresponding to the titrations of FAM-labeled BubR1$^{392-425}$ (*black*), BubR1$^{400-425}$ (*green*), BubR1$^{392-419}$ (*blue*), and BubR1$^{400-419}$ (*red*) on 2.5 nM GST-Bub3 labeled with an anti-GST Tb3+ conjugate antibody. Fitting of the data to a one-site specific binding model (*lines*) generated the K_D values shown in Table 1. *C*, inhibition curves resulting from the titration of untagged BubR1$^{392-425}$ (*black*), BubR1$^{400-425}$ (*green*), BubR1$^{392-419}$ (*blue*), and BubR1$^{400-419}$ (*red*) at the concentration indicated in a mix of 3 nM FAM-BubR1$^{392-425}$ and 2.5 nM of GST-Bub3 labeled as described above. Fitting of the data to a competitive binding model (*lines*) resulted in the K_i values shown in Table 1. *D*, TSA thermal denaturation curves corresponding to His-Bub3 alone (*gray*) and in combination with 10-fold molar excess of untagged BubR1$^{392-425}$ (*black*), BubR1$^{400-425}$ (*green*), BubR1$^{392-419}$ (*blue*), and BubR1$^{400-419}$ (*red*). Analysis of these melting curves with a first derivative method delivered the corresponding T_m values that were used to calculate the shifts (ΔT_m) shown in Table 1. *RFU*, relative fluorescence units.

with a ΔH and a $-T\Delta S$ of -2.7 ± 0.2 and -5.6 kcal·mol^{-1}, respectively. The low binding enthalpy of this peptide fragment indicates the hydrogen bonds established by its amino acids contribute only a minor part of the enthalpic interactions made by the extended fragment BubR1$^{392-425}$. Also for these variants, the stoichiometry was 1:1, and the overall affinity ranking obtained with ITC is in agreement with those measured with TR-FRET and SPR.

Effects of the Inhibition of the Human BubR1·Bub3 Interaction by the GLEBS Domain in Vitro and in Cells—Having extensively characterized the interaction of human Bub3 and the BubR1 GLEBS motif, we next asked whether other structural elements in BubR1 also contribute significantly to the recognition between the proteins. To address this question, we expressed recombinant full-length BubR1 (BubR1FL) in-frame with a GST tag and performed TR-FRET saturation binding and competition experiments (Fig. 6, *A* and *B*) similar to those shown above for the GLEBS domain. Under these conditions, BubR1^{FL} interacted with Bub3 with similar affinity (1.19 ± 0.4 nM; Fig. 6*A*) as the GLEBS fragment (2.12 ± 0.3 nM; Fig. 3*A*). Moreover, the binding of full-length BubR1 and Bub3 was outcompeted by untagged BubR1$^{364-384}$

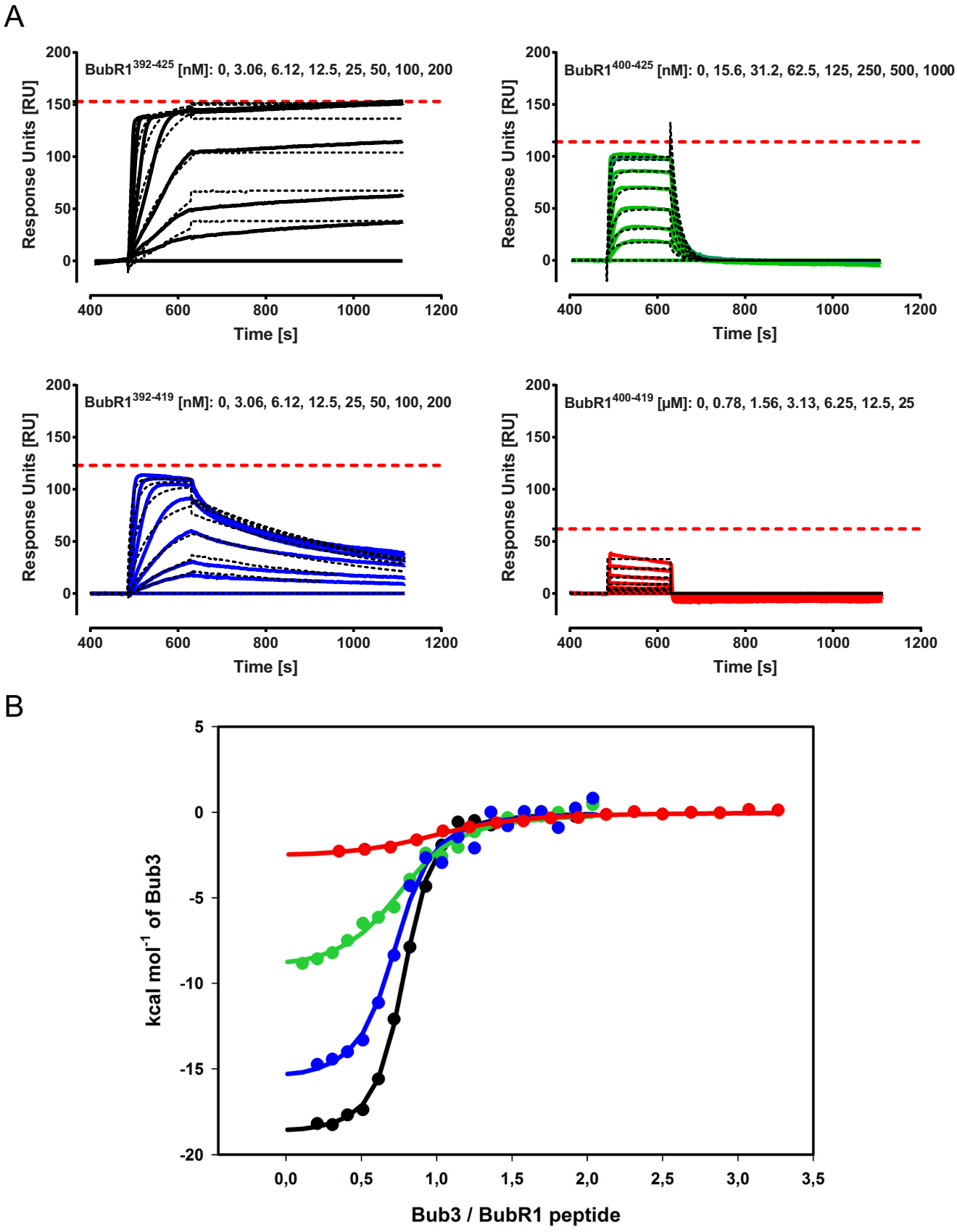
A
BubR1392-425 [nM]: 0, 3.06, 6.12, 12.5, 25, 50, 100, 200
BubR1400-425 [nM]: 0, 15.6, 31.2, 62.5, 125, 250, 500, 1000
BubR1392-419 [nM]: 0, 3.06, 6.12, 12.5, 25, 50, 100, 200
BubR1400-419 [μM]: 0, 0.78, 1.56, 3.13, 6.25, 12.5, 25
Response Units [RU]
Time [s]
B
kcal mol-1 of Bub3
Bub3 / BubR1 peptide

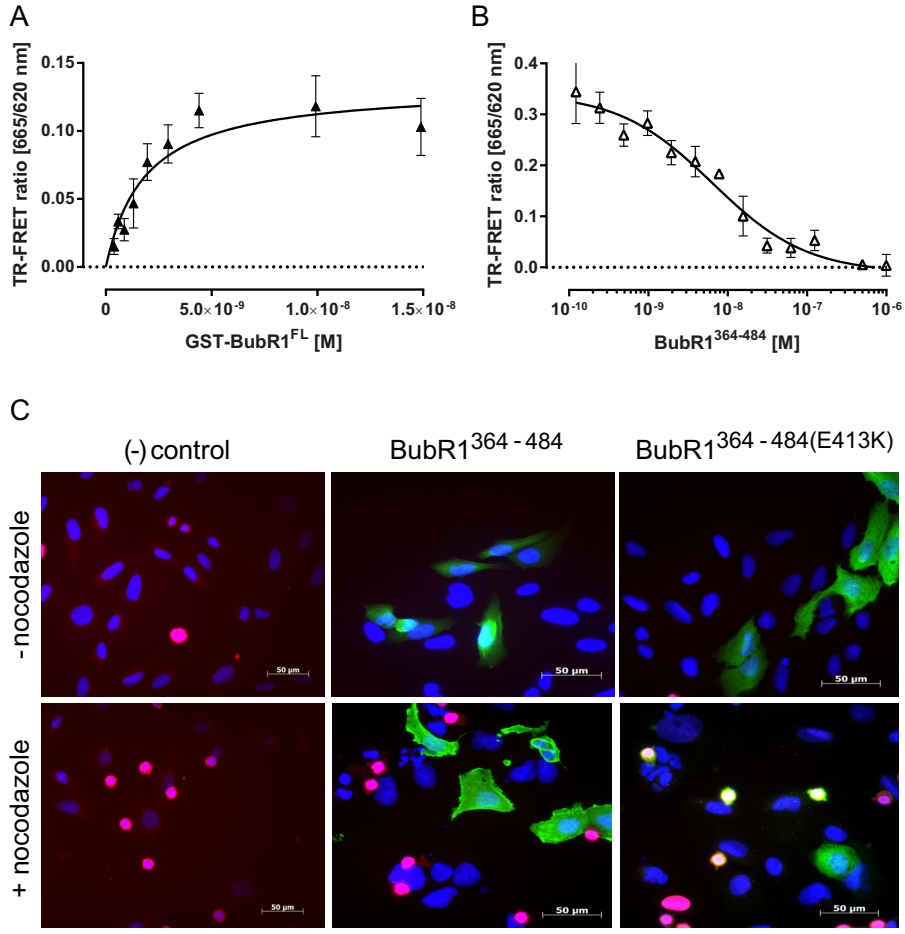

FIGURE 6. **Effect of inhibiting Bub3 interactions with BubR1 *in vitro* and in human cells.** *A*, TR-FRET saturation binding curve corresponding to the titrations of GST-BubR1^{FL} at the concentrations indicated on 1 nM His-Bub3. BubR1 was labeled with anti-GST-XL665 and Bub3 with an anti-His Eu^{3+} cryptate conjugate. Fitting of the data to a one-site specific binding model (*lines*) generated the K_D value indicated in Table 1. *B*, TR-FRET inhibition curve resulting from the titration of untagged BubR1$^{364-484}$ at the concentration indicated into a mixture of 1.5 nM GST-BubR1^{FL} and 1 nM His-Bub3 labeled as described above. Fitting of the data to a competitive binding model (*lines*) resulted in the K_i value described under "Results." *C*, representative fluorescence microscopy images of U2-OS cells transfected with V5-BubR1 GLEBS domain variants without (−) or with (+) 16 h of nocodazole treatment and stained with anti V5 antibody (*green*), phosphohistone H3 antibody (*red*), and Hoechst 33342 (*blue*).

with a K_i of 3.33 ± 0.6 nM (Fig. 6*B*). This is in a similar order of magnitude to the K_D of the interaction and means that the saturation binding experiment was not biased by unspecific binding of the fluorescent labeling or by titration of the detection system. Similar results were obtained when an unlabeled BubR1$^{392-425}$ peptide was used as a competitor in the same experiments (data not shown).

These findings showed that the affinity of full-length BubR1 for Bub3 is predominantly determined by its GLEBS motif and encouraged us to ask whether it would be possible to inhibit the SAC by inhibiting the endogenous human Bub3 and BubR1 interaction in living cells. To address this question we transfected cultured human U2-OS cells with DNA plasmids encoding either the V5-tagged BubR1 GLEBS domain (amino acids 364–484) WT or two point mutants thereof (E409K and E413K, respectively). Fluorescence microscopy analysis of these cells (Fig. 6*C*) showed that although nocodazole treatment resulted in prometaphase arrest phenotype (many rounded cells) upon transfection with the mutant GLEBS (shown for the mutant E413K; similar results with E409K, not shown), only a few of these rounded cells were observed after transfection with the wild type GLEBS domain (SAC inhibition phenotype). A similar effect was observed upon the expression of WT and mutated human BubR1$^{50-486}$, respectively (not shown). Furthermore, the human BubR1 fragments could also be replaced by their murine counterparts (not shown). We tried to further narrow down the size of the GLEBS peptides required for Bub3 inhibition in cells but (in contrast to previous reports

FIGURE 5. **Kinetics and thermodynamics parameters for the interaction of human Bub3 and BubR1 GLEBS variants.** *A*, SPR sensorgrams corresponding to the titration of untagged BubR1$^{392-425}$ (*black*), BubR1$^{400-425}$ (*green*), BubR1$^{392-419}$ (*blue*), and BubR1$^{400-419}$ (*red*) peptides at the indicated concentrations, on a Ni-NTA sensor chip coated with His-tagged Bub3. *Red dotted lines* represent the theoretical Rmax of a 1:1 interaction, assuming 100% binding activity of both interaction partners. Fitting of the kinetic traces to Langmuir 1:1 interaction model delivered the parameters specified in Table 1. To obtain the equilibrium $K_{D\,eq}$ values (Table 1), steady state response units were plotted *versus* the concentrations of BubR1 and fitted to a single site binding model. *B*, ITC titrations of BubR1 peptides with Bub3 at 25 °C. Clockwise, 7 μM BubR1$^{392-425}$ was titrated with 70 μM GST-Bub3 (fit shown in *black*), 7 μM BubR1$^{400-425}$ was titrated with 70 μM GST-Bub3 (fit shown in *green*), 10 μM BubR1$^{392-419}$ was titrated with 170 μM GST-Bub3 (fit shown in *blue*), and 7 μM BubR1$^{400-419}$ was titrated with 70 μM GST-Bub3 (fit shown in *red*). Data were fitted to a single-site binding model to obtain thermodynamic parameters shown in Table 1.

on murine BubR1-GLEBS; Ref. 31) failed to express a shorter human BubR1 version, possibly due to misfolding and degradation of the short fragment.

These results demonstrate that Bub3 binding to BubR1 is essential for correct SAC signaling in human cells and suggest that disrupting this interaction with appropriate, cell-permeable biological or chemical agents could also be a strategy to inhibit the SAC.

Discussion

The SAC plays an indispensable role for the cell to ensure faithful distribution of daughter chromosomes during mitosis. It has been suggested that SAC weakening or abrogation results in polyploidy or aneuploidy and could promote tumorigenesis. Indeed, most tumor cells display certain levels of chromosomal instability. On the other hand, mutations in mitotic checkpoint genes are not frequent in tumors, and the proteins are often even up-regulated in tumors. Therefore, it has been proposed that the SAC might represent an attractive target for targeted tumor therapy, and drug discovery projects for SAC inhibitors have been initiated, *e.g.* Mps1 inhibitors (1, 32, 33).

Our results further support the SAC and more specifically Bub3 as a target for tumor therapy. Bub3 depletion results in reduced proliferation and induction of apoptosis in several tumor cell lines, whereas Hs68 and primary human fibroblasts are virtually unaffected. Intriguingly, Hs68 and primary fibroblasts survive long term knockdown of Bub3 and are viable with as little as 20% remaining Bub3 levels. On the contrary, long term knockdown of Bub3 in several tumor cells resulted in the outgrowth of few surviving and clonally outgrowing cells. Determination of the remaining Bub3 protein levels in tumor cell lines showed unaltered or even slightly increased Bub3 protein levels as compared with control shRNAs. The slight increase of Bub3 protein might be caused by the high rate of proliferation of the clonal cells. These results suggest that tumor cells with an efficient Bub3 knockdown were lost during the course of the experiment, whereas the only surviving cells were those that expressed the resistance marker but did not show a strong Bub3 knockdown. These results are in line with the observation that a functional SAC seems to be essential for tumor cells, and expression levels for Mps1 frequently are increased in tumors (34–37).

$Bub3^{-/-}$ mice are not viable beyond day 6.5–7.5 post coitus (5, 6), indicating that residual Bub3 levels are essential for cell survival. On the other hand, $Bub3^{+/-}$ haplo-insufficiency only results in aneuploidy. Spontaneous tumor formation is not accelerated; however, these animals are more susceptible to chemical carcinogenesis (19). Finally, aneuploidy progresses with age and is accelerated in $Bub3^{+/-}$/$Rae1^{+/-}$ dual haplo-insufficient animals (20). A similar phenotype was observed with gradual BubR1 reduction, resulting in progressively more aneuploidy and senescence in mouse embryonic fibroblasts, an early aging phenotype in mice and increased sensitivity toward chemical carcinogenesis (7, 38). Taken together, these published results and our results suggest that non-transformed cells can cope with some degree of SAC impairment. Additional stress like carcinogen exposure, higher rates of proliferation, increased replicative stress, or existing aneuploidy could overburden the weakened checkpoint, resulting in tumor formation in checkpoint-impaired animals and death of tumor cell. Collectively, we conclude an increased sensitivity of tumor cells as compared with non-transformed cells, further supporting the SAC as a valid and selective target for cancer therapy.

It has previously been shown that the amino acids Arg-197 in yeast Bub3 and Glu-409 and Glu-413 in human BubR1 are critical residues for the interaction between these proteins (16–18, 39). With our homology model we predicted *S. cerevisiae* $Bub3_{Arg\text{-}197}$ to be equivalent to human $Bub3_{Arg\text{-}183}$. Using immunoprecipitation experiments, we could re-confirm the relevance of these residues in a human setting as single point mutations (switching Glu to Lys and Arg to Glu, respectively) completely abolished the interaction between Bub3 and BubR1 after transfection of the respective-tagged constructs into cells.

Next we conducted a detailed quantitative analysis of the interaction between human Bub3 and BubR1. To our knowledge this is the first time affinity measurements are made using the two full-length proteins. Comparison of the K_D values measured for $BubR1^{FL}$ with those of $BubR1^{364-484}$ and $BubR1^{392-425}$ suggests that $BubR1^{392-425}$ is the minimum fragment required to achieve maximum binding efficiency of BubR1 to Bub3. The affinities measured with different methods for all three variants were surprisingly high, pointing to a much tighter interaction in humans as compared with *S. cerevisiae*, where ITC measurements of Bub3 binding to Mad3 (the yeast homologue of BubR1) and Bub1 peptides yielded K_D values in the low micromolar range (17). Interestingly, Bub3 is not essential for SAC activity in yeast (40, 41), and high affinity binding interaction of Mad3 and Bub3 might not be required for high fidelity of SAC function.

Of note, our K_D values obtained from kinetic measurements were 10-fold lower than the same parameter estimated with steady state methods, suggesting that the interaction could be even tighter. Unfortunately the accuracy of the SPR kinetic parameters is limited by the assay configuration (non-covalently captured target) and, potentially, mass transport effects (42). Otherwise, one could argue that due to the slow kinetics of the interaction, the steady state K_D values are underestimated because equilibrium is not achieved for all concentrations tested in the time of the respective experiments. This was obviously the case for the SPR steady state analysis of full-length and N-terminal-deleted GLEBS peptides.

Besides defining the amino acids 392–425 of the GLEBS peptide as the minimal Bub3 binding fragment in BubR1, we have been able to link the affinity, kinetics, and thermodynamics of the interaction to defined structural features in this motif. For instance, one interesting observation from our study is the non-diffusion controlled kinetics of the association between BubR1 GLEBS ($BubR1^{364-484}$) and Bub3. Similar findings have been reported for the interaction of two other MCC components: O-MAD2 and CDC20 (43). This implies that (as k_{on} is a concentration-dependent, second order rate constant) achieving full recruitment in a biologically relevant time frame requires at least one of the proteins to be in concentrations far above the K_D of the interaction. Alternatively accessory proteins would be necessary to modulate the kinetics of this binding event.

With regard to the dissociation kinetics, the half-life of the BubR1·Bub3 complexes exceeds by far the duration of mitosis, indicating that they are de facto irreversible until degradation by the APC/C takes place. This tight interaction is in agreement with recent size exclusion chromatography studies in which both human proteins co-elute in the same fraction as long as the GLEBS motif of BubR1 is present (39). To permit fine-tuning or shutdown of the activated SAC, it is tempting to postulate additional means of weakening of the complex, *e.g.* by the interaction with MCC components, by additional regulatory proteins or post-translational modifications. Also noteworthy is that our results indicate that the contacts established by the conserved Met-397, Tyr-398, and Cys-399 are more relevant for the dissociation rate of the interactions than those made by Glu-409 and Glu-413. Interestingly, in lower organisms such as *Drosophila melanogaster* and *S. cerevisiae* with shorter mitosis times than *H. sapiens*, the degree of conservation of Met-397 and Cys-399 is the lowest, whereas Glu-409 and Glu-413 are conserved through all species.

The thermodynamic analysis of the binding of human BubR1 to Bub3 points also to a 1:1 stoichiometry of the interaction, with a nanomolar affinity. The substantial binding enthalpy is a frequently observed property of high affinity linear peptides interacting with protein domains (for example, see Refs. 44–46) and is consistent with a net increase in non-covalent bond formation associated with the ordering of the peptide upon protein engagement. The use of thermal shift assays to characterize protein-protein interactions is becoming an interesting topic (47, 48), and here we show a further example of the potential of the method.

Based on our results, a hypothesis about the possible mechanism of molecular recognition between BubR1 and Bub3 could be elaborated; for instance, the fact that Glu-409 and Glu-413 are indispensable for the binding of the 33-amino acid GLEBS peptide contrasts with the observation that a 19-amino acid truncated version of it retains only a small fraction of the binding affinity. More interesting, the binding of this peptide to Bub3 is diffusion-controlled and, with both enthalpic and entropic contributions, probably driven by the establishment of the Glu-409 and Glu-413 salt bridges and hydrophobic contacts in the funnel region. This could be the first step of the cooperative recognition between the two molecules followed by small rearrangements in Bub3 loop regions, which might be required to accommodate the C-terminal part of the peptide. This step is not diffusion-controlled but is relatively fast and, in contrast to the first, has a relatively short half-life. Finally, several important contacts must be made between the N-terminal part of the BubR1 peptide and another loop of Bub3, which in addition may go through more important conformational changes. This anchoring step takes place at a high entropy cost but is compensated by an even higher enthalpy contribution and would be to a great extent responsible for the long half-life of the BubR1·Bub3 interaction.

In future work it would be interesting to investigate the kinetics and thermodynamics of the interaction of the full-length proteins as well as in the presence of other members of the MCC. In this direction, recently published work reported interesting results in which Bub1·Bub3·MELT trimolecular complexes were measured using ITC (15).

In this study we were able to "therapeutically" override the SAC in cancer cells despite the presence of endogenous Bub1 and BubR1. We speculate that we blocked most of the intracellular Bub3 by overexpression of BubR1 GLEBS, thus abolishing all Bub3 funnel interactions. Therefore, we are not able to distinguish between the individual contributions of Bub1 and BubR1 to the observed phenotype. Subsequent studies will further elucidate the individual roles of Bub1 and BubR1. In any case these results confirmed in human cells earlier observations with murine counterparts (31, 49), indicating that blockage of the interaction between Bub3 and their binding partners Bub1 and BubR1 is sufficient for checkpoint inhibition. The latter is in line with very recent publications (18, 39) showing that expression of wild type, but not mutated or truncated BubR1 GLEBS, could rescue the SAC in BubR1-depleted cells, although the p53 status might influence the SAC response (50).

From a chemical biology and drug discovery standpoint, our results combined with structural information could be of relevance for the identification of "hot spots" (51) or "hot segments" (52) for the Bub3·BubR1 protein-protein interaction, which in turn could lead to the design of small molecule inhibitors targeting it. The biochemical and biophysical assays described in this work can be useful for this purpose as well as for the screening of chemical libraries. To date, several examples of small molecules binding to WD40 proteins have been described, *e.g.* targeting $G\beta\gamma$, WDR5, or CDC20 (53–58), meaning that such an endeavor could be rewarding in the case of Bub3. Of note, the first small molecule inhibitor targeting the WDR5-MLL protein-protein interaction by blocking the funnel of the WD40 protein WDR5 has been recently published (54, 55) indicating that this might be a generally applicable principle. Along these lines, here we have devised a cellular system to investigate the feasibility and biological effects of putative Bub3 inhibitors in human tumor cells. Without potent and specific compounds at hand, we were able to validate this assay by overexpressing a BubR1 GLEBS.

Altogether, our results along with multiple reports of a weakened SAC in tumor cells and an increased dependence of tumor cells on a functional SAC (1, 28, 29, 32, 33) support the SAC and its components (in this case Bub3) as promising targets for cancer therapy. Until small molecule Bub3 inhibitors become available, alternative strategies based on the GLEBS sequence, such as cell penetrating therapeutic peptides (59) or gene therapy approaches, could be envisioned. Ideally the present work will inspire further studies on the BubR1·Bub3 interaction and the development of novel cancer therapeutics targeting the SAC.

Author Contributions—F. P., S. J. H., G. B., B. K., and A. F.-M. conceived the study. F. P., V. P., S. J. H., D. A., D. K., C. M. S., S. P., G. B., B. K., and A. F.-M. contributed to the design and acquisition of data. F. P., V. P., S. J. H., D. A., C. M. S., B. K., and A. F.-M. contributed to the analysis and interpretation of data. F. P., V. P., S. J. H., K. P., and A. F.-M. drafted the manuscript F. P., S. J. H., C. M. S., D. M., and A. F.-M. critically revised the manuscript for important intellectual content. All authors gave final approval of the version to be published.

Acknowledgments—We thank Drs. Karsten Parczyk and Anke Müller-Fahrnow for critical reading of the manuscript. We acknowledge Franziska Bockhardt, Nicole Dittmar, Roopa Jayarama-Naidu, Jane Beschorner, and Carolin Pohle for excellent technical support.

References

1. Jemaà, M., Galluzzi, L., Kepp, O., Senovilla, L., Brands, M., Boemer, U., Koppitz, M., Lienau, P., Prechtl, S., Schulze, V., Siemeister, G., Wengner, A. M., Mumberg, D., Ziegelbauer, K., Abrieu, A., Castedo, M., Vitale, I., and Kroemer, G. (2013) Characterization of novel MPS1 inhibitors with preclinical anticancer activity. *Cell Death Differ.* **20,** 1532–1545
2. Sudakin, V., Chan, G. K., and Yen, T. J. (2001) Checkpoint inhibition of the APC/C in HeLa cells is mediated by a complex of BUBR1, BUB3, CDC20, and MAD2. *J. Cell Biol.* **154,** 925–936
3. Tang, Z., Bharadwaj, R., Li, B., and Yu, H. (2001) Mad2-Independent inhibition of APCCdc20 by the mitotic checkpoint protein BubR1. *Dev. Cell* **1,** 227–237
4. Dobles, M., Liberal, V., Scott, M. L., Benezra, R., and Sorger, P. K. (2000) Chromosome missegregation and apoptosis in mice lacking the mitotic checkpoint protein Mad2. *Cell* **101,** 635–645
5. Kalitsis, P., Earle, E., Fowler, K. J., and Choo, K. H. (2000) Bub3 gene disruption in mice reveals essential mitotic spindle checkpoint function during early embryogenesis. *Genes Dev.* **14,** 2277–2282
6. Babu, J. R., Jeganathan, K. B., Baker, D. J., Wu, X., Kang-Decker, N., and van Deursen, J. M. (2003) Rae1 is an essential mitotic checkpoint regulator that cooperates with Bub3 to prevent chromosome missegregation. *J. Cell Biol.* **160,** 341–353
7. Baker, D. J., Jeganathan, K. B., Cameron, J. D., Thompson, M., Juneja, S., Kopecka, A., Kumar, R., Jenkins, R. B., de Groen, P. C., Roche, P., and van Deursen, J. M. (2004) BubR1 insufficiency causes early onset of aging-associated phenotypes and infertility in mice. *Nat. Genet.* **36,** 744–749
8. Larsen, N. A., and Harrison, S. C. (2004) Crystal structure of the spindle assembly checkpoint protein Bub3. *J. Mol. Biol.* **344,** 885–892
9. Wilson, D. K., Cerna, D., and Chew, E. (2005) The 1.1-angstrom structure of the spindle checkpoint protein Bub3p reveals functional regions. *J. Biol. Chem.* **280,** 13944–13951
10. Kiyomitsu, T., Obuse, C., and Yanagida, M. (2007) Human Blinkin/AF15q14 is required for chromosome alignment and the mitotic checkpoint through direct interaction with Bub1 and BubR1. *Dev. Cell* **13,** 663–676
11. Krenn, V., Wehenkel, A., Li, X., Santaguida, S., and Musacchio, A. (2012) Structural analysis reveals features of the spindle checkpoint kinase Bub1-kinetochore subunit Knl1 interaction. *J. Cell Biol.* **196,** 451–467
12. London, N., Ceto, S., Ranish, J. A., and Biggins, S. (2012) Phosphoregulation of Spc105 by Mps1 and PP1 regulates Bub1 localization to kinetochores. *Curr. Biol.* **22,** 900–906
13. Shepperd, L. A., Meadows, J. C., Sochaj, A. M., Lancaster, T. C., Zou, J., Buttrick, G. J., Rappsilber, J., Hardwick, K. G., and Millar, J. B. (2012) Phospho-dependent recruitment of Bub1 and Bub3 to Spc7/KNL1 by Mph1 kinase maintains the spindle checkpoint. *Curr. Biol.* **22,** 891–899
14. Yamagishi, Y., Yang, C. H., Tanno, Y., and Watanabe, Y. (2012) MPS1/Mph1 phosphorylates the kinetochore protein KNL1/Spc7 to recruit SAC components. *Nat. Cell Biol.* **14,** 746–752
15. Primorac, I., Weir, J. R., Chiroli, E., Gross, F., Hoffmann, I., van Gerwen, S., Ciliberto, A., and Musacchio, A. (2013) Bub3 reads phosphorylated MELT repeats to promote spindle assembly checkpoint signaling. *eLife* **2,** e01030
16. Taylor, S. S., Ha, E., and McKeon, F. (1998) The human homologue of Bub3 is required for kinetochore localization of Bub1 and a Mad3/Bub1-related protein kinase. *J. Cell Biol.* **142,** 1–11
17. Larsen, N. A., Al-Bassam, J., Wei, R. R., and Harrison, S. C. (2007) Structural analysis of Bub3 interactions in the mitotic spindle checkpoint. *Proc. Natl. Acad. Sci. U.S.A.* **104,** 1201–1206
18. Han, J. S., Vitre, B., Fachinetti, D., and Cleveland, D. W. (2014) Bimodal activation of BubR1 by Bub3 sustains mitotic checkpoint signaling. *Proc. Natl. Acad. Sci. U.S.A.* **111,** E4185–E4193
19. Kalitsis, P., Fowler, K. J., Griffiths, B., Earle, E., Chow, C. W., Jamsen, K., and Choo, K. H. (2005) Increased chromosome instability but not cancer predisposition in haploinsufficient Bub3 mice. *Genes Chromosomes Cancer* **44,** 29–36
20. Baker, D. J., Jeganathan, K. B., Malureanu, L., Perez-Terzic, C., Terzic, A., and van Deursen, J. M. (2006) Early aging-associated phenotypes in Bub3/Rae1 haploinsufficient mice. *J. Cell Biol.* **172,** 529–540
21. Wang, X., Babu, J. R., Harden, J. M., Jablonski, S. A., Gazi, M. H., Lingle, W. L., de Groen, P. C., Yen, T. J., and van Deursen, J. M. (2001) The mitotic checkpoint protein hBUB3 and the mRNA export factor hRAE1 interact with GLE2p-binding sequence (GLEBS)-containing proteins. *J. Biol. Chem.* **276,** 26559–26567
22. Livak, K. J., and Schmittgen, T. D. (2001) Analysis of relative gene expression data using real-time quantitative PCR and the $2(-\Delta\Delta CT)$ method. *Methods* **25,** 402–408
23. Cheng, Y., and Prusoff, W. H. (1973) Relationship between the inhibition constant (K1) and the concentration of inhibitor which causes 50 per cent inhibition (I_{50}) of an enzymatic reaction. *Biochem. Pharmacol.* **22,** 3099–3108
24. Nieba, L., Nieba-Axmann, S. E., Persson, A., Hämäläinen, M., Edebratt, F., Hansson, A., Lidholm, J., Magnusson, K., Karlsson, A. F., and Plückthun, A. (1997) BIACORE analysis of histidine-tagged proteins using a chelating NTA sensor chip. *Anal. Biochem.* **252,** 217–228
25. Hutsell, S. Q., Kimple, R. J., Siderovski, D. P., Willard, F. S., and Kimple, A. J. (2010) High-affinity immobilization of proteins using biotin- and GST-based coupling strategies. *Methods Mol. Biol.* **627,** 75–90
26. Karlsson, R., Katsamba, P. S., Nordin, H., Pol, E., and Myszka, D. G. (2006) Analyzing a kinetic titration series using affinity biosensors. *Anal. Biochem.* **349,** 136–147
27. Logarinho, E., and Bousbaa, H. (2008) Kinetochore-microtubule interactions "in check" by Bub1, Bub3 and BubR1: the dual task of attaching and signalling. *Cell Cycle* **7,** 1763–1768
28. Kops, G. J., Weaver, B. A., and Cleveland, D. W. (2005) On the road to cancer: aneuploidy and the mitotic checkpoint. *Nat. Rev. Cancer* **5,** 773–785
29. Manchado, E., Guillamot, M., and Malumbres, M. (2012) Killing cells by targeting mitosis. *Cell Death Differ.* **19,** 369–377
30. Rich, R. L., and Myszka, D. G. (2000) Advances in surface plasmon resonance biosensor analysis. *Curr. Opin. Biotechnol.* **11,** 54–61
31. Harris, L., Davenport, J., Neale, G., and Goorha, R. (2005) The mitotic checkpoint gene BubR1 has two distinct functions in mitosis. *Exp. Cell Res.* **308,** 85–100
32. Slee, R. B., Grimes, B. R., Bansal, R., Gore, J., Blackburn, C., Brown, L., Gasaway, R., Jeong, J., Victorino, J., March, K. L., Colombo, R., Herbert, B. S., and Korc, M. (2014) Selective inhibition of pancreatic ductal adenocarcinoma cell growth by the mitotic MPS1 kinase inhibitor NMS-P715. *Mol. Cancer Ther.* **13,** 307–315
33. Jemaà, M., Vitale, I., Kepp, O., Berardinelli, F., Galluzzi, L., Senovilla, L., Mariño, G., Malik, S. A., Rello-Varona, S., Lissa, D., Antoccia, A., Tailler, M., Schlemmer, F., Harper, F., Pierron, G., Castedo, M., and Kroemer, G. (2012) Selective killing of p53-deficient cancer cells by SP600125. *EMBO Mol. Med.* **4,** 500–514
34. Yuan, B., Xu, Y., Woo, J. H., Wang, Y., Bae, Y. K., Yoon, D. S., Wersto, R. P., Tully, E., Wilsbach, K., and Gabrielson, E. (2006) Increased expression of mitotic checkpoint genes in breast cancer cells with chromosomal instability. *Clin. Cancer Res.* **12,** 405–410
35. Daniel, J., Coulter, J., Woo, J. H., Wilsbach, K., and Gabrielson, E. (2011) High levels of the Mps1 checkpoint protein are protective of aneuploidy in breast cancer cells. *Proc. Natl. Acad. Sci. U.S.A.* **108,** 5384–5389
36. Weaver, B. A., and Cleveland, D. W. (2006) Does aneuploidy cause cancer? *Curr. Opin. Cell Biol.* **18,** 658–667
37. Salvatore, G., Nappi, T. C., Salerno, P., Jiang, Y., Garbi, C., Ugolini, C., Miccoli, P., Basolo, F., Castellone, M. D., Cirafici, A. M., Melillo, R. M., Fusco, A., Bittner, M. L., and Santoro, M. (2007) A cell proliferation and chromosomal instability signature in anaplastic thyroid carcinoma. *Cancer Res.* **67,** 10148–10158
38. Dai, W., Wang, Q., Liu, T., Swamy, M., Fang, Y., Xie, S., Mahmood, R., Yang, Y. M., Xu, M., and Rao, C. V. (2004) Slippage of mitotic arrest and

enhanced tumor development in mice with BubR1 haploinsufficiency. *Cancer Res.* **64,** 440–445
39. Overlack, K., Primorac, I., Vleugel, M., Krenn, V., Maffini, S., Hoffmann, I., Kops, G. J., and Musacchio, A. (2015) A molecular basis for the differential roles of Bub1 and BubR1 in the spindle assembly checkpoint. *eLife* **4,** e05269
40. Windecker, H., Langegger, M., Heinrich, S., and Hauf, S. (2009) Bub1 and Bub3 promote the conversion from monopolar to bipolar chromosome attachment independently of shugoshin. *EMBO Rep.* **10,** 1022–1028
41. Tange, Y., and Niwa, O. (2008) *Schizosaccharomyces pombe* Bub3 is dispensable for mitotic arrest following perturbed spindle formation. *Genetics* **179,** 785–792
42. Myszka, D. G., He, X., Dembo, M., Morton, T. A., and Goldstein, B. (1998) Extending the range of rate constants available from BIACORE: interpreting mass transport-influenced binding data. *Biophys. J.* **75,** 583–594
43. Musacchio, A., and Salmon, E. D. (2007) The spindle-assembly checkpoint in space and time. *Nat. Rev. Mol. Cell Biol.* **8,** 379–393
44. O'Brien, R., Rugman, P., Renzoni, D., Layton, M., Handa, R., Hilyard, K., Waterfield, M. D., Driscoll, P. C., and Ladbury, J. E. (2000) Alternative modes of binding of proteins with tandem SH2 domains. *Protein Sci.* **9,** 570–579
45. Stolt, P. C., Vardar, D., and Blacklow, S. C. (2004) The dual-function disabled-1 PTB domain exhibits site independence in binding phosphoinositide and peptide ligands. *Biochemistry* **43,** 10979–10987
46. Hahn, M., Winkler, D., Welfle, K., Misselwitz, R., Welfle, H., Wessner, H., Zahn, G., Scholz, C., Seifert, M., Harkins, R., Schneider-Mergener, J., and Höhne, W. (2001) Cross-reactive binding of cyclic peptides to an anti-TGFα antibody Fab fragment: an x-ray structural and thermodynamic analysis. *J. Mol. Biol.* **314,** 293–309
47. Layton, C. J., and Hellinga, H. W. (2011) Quantitation of protein-protein interactions by thermal stability shift analysis. *Protein Sci.* **20,** 1439–1450
48. Chari, A., Haselbach, D., Kirves, J. M., Ohmer, J., Paknia, E., Fischer, N., Ganichkin, O., Möller, V., Frye, J. J., Petzold, G., Jarvis, M., Tietzel, M., Grimm, C., Peters, J. M., Schulman, B. A., Tittmann, K., Markl, J., Fischer, U., and Stark, H. (2015) ProteoPlex: stability optimization of macromolecular complexes by sparse-matrix screening of chemical space. *Nat. Methods* **12,** 859–865
49. Davenport, J., Harris, L. D., and Goorha, R. (2006) Spindle checkpoint function requires Mad2-dependent Cdc20 binding to the Mad3 homology domain of BubR1. *Exp. Cell Res.* **312,** 1831–1842
50. Malureanu, L. A., Jeganathan, K. B., Hamada, M., Wasilewski, L., Davenport, J., and van Deursen, J. M. (2009) BubR1 N terminus acts as a soluble inhibitor of cyclin B degradation by APC/C(Cdc20) in interphase. *Dev. Cell* **16,** 118–131
51. Wells, J. A., and McClendon, C. L. (2007) Reaching for high-hanging fruit in drug discovery at protein-protein interfaces. *Nature* **450,** 1001–1009
52. London, N., Raveh, B., and Schueler-Furman, O. (2013) Druggable protein-protein interactions: from hot spots to hot segments. *Curr. Opin. Chem. Biol.* **17,** 952–959
53. Bonacci, T. M., Mathews, J. L., Yuan, C., Lehmann, D. M., Malik, S., Wu, D., Font, J. L., Bidlack, J. M., and Smrcka, A. V. (2006) Differential targeting of G$\beta\gamma$-subunit signaling with small molecules. *Science* **312,** 443–446
54. Bolshan, Y., Getlik, M., Kuznetsova, E., Wasney, G. A., Hajian, T., Poda, G., Nguyen, K. T., Wu, H., Dombrovski, L., Dong, A., Senisterra, G., Schapira, M., Arrowsmith, C. H., Brown, P. J., Al-Awar, R., Vedadi, M., and Smil, D. (2013) Synthesis, optimization, and evaluation of novel small molecules as antagonists of WDR5-MLL interaction. *ACS Med. Chem. Lett.* **4,** 353–357
55. Senisterra, G., Wu, H., Allali-Hassani, A., Wasney, G. A., Barsyte-Lovejoy, D., Dombrovski, L., Dong, A., Nguyen, K. T., Smil, D., Bolshan, Y., Hajian, T., He, H., Seitova, A., Chau, I., Li, F., Poda, G., Couture, J. F., Brown, P. J., Al-Awar, R., Schapira, M., Arrowsmith, C. H., and Vedadi, M. (2013) Small-molecule inhibition of MLL activity by disruption of its interaction with WDR5. *Biochem. J.* **449,** 151–159
56. Karatas, H., Townsend, E. C., Cao, F., Chen, Y., Bernard, D., Liu, L., Lei, M., Dou, Y., and Wang, S. (2013) High-affinity, small-molecule peptidomimetic inhibitors of MLL1/WDR5 protein-protein interaction. *J. Am. Chem. Soc.* **135,** 669–682
57. Grebien, F., Vedadi, M., Getlik, M., Giambruno, R., Grover, A., Avellino, R., Skucha, A., Vittori, S., Kuznetsova, E., Smil, D., Barsyte-Lovejoy, D., Li, F., Poda, G., Schapira, M., Wu, H., *et al.* (2015) Pharmacological targeting of the Wdr5-MLL interaction in C/EBPα N-terminal leukemia. *Nat. Chem. Biol.* **11,** 571–578
58. Sackton, K. L., Dimova, N., Zeng, X., Tian, W., Zhang, M., Sackton, T. B., Meaders, J., Pfaff, K. L., Sigoillot, F., Yu, H., Luo, X., and King, R. W. (2014) Synergistic blockade of mitotic exit by two chemical inhibitors of the APC/C. *Nature* **514,** 646–649
59. Verdine, G. L., and Hilinski, G. J. (2012) Stapled peptides for intracellular drug targets. *Methods Enzymol.* **503,** 3–33